Membrane Protein Modification Modulates Big and Small Extracellular Vesicle Biodistribution and Tumorigenic Potential in Breast Cancers *In Vivo*

*Bryan John Abel Magoling, Yen-Ju Chen, Anthony Yan-Tang Wu, Wendy Wan-Ting Wong, Steven Ting-Yu Chuo, Hsi-Chien Huang, Yun-Chieh Sung, Hsin Tzu Hsieh, Poya Huang, Kang-Zhang Lee, Kuan-Wei Huang, Ruey-Hwa Chen, Yunching Chen, Charles Pin-Kuang Lai**

B.J.A. Magoling, Y.-J. Chen, A.Y.-T. Wu, W.W.-T. Wong, S.T.-Y. Chuo, P. Huang, K.-Z. Lee, C.P.-K. Lai
Institute of Atomic and Molecular Sciences, Academia Sinica, Taipei, 10617 Taiwan
E-mail: laicharles@sinica.edu.tw

B.J.A. Magoling, R.-H. Chen
Graduate Institute of Biochemical Sciences, National Taiwan University, Taipei, 10617 Taiwan

B.J.A. Magoling, A.Y.-T. Wu, R.-H. Chen, C.P.-K. Lai
Chemical Biology and Molecular Biophysics Program, TIGP, Academia Sinica, Taipei, 11529 Taiwan

A Y.-T. Wu
Department of Pharmacology, College of Medicine, National Taiwan University, Taipei, 100233 Taiwan

R.-H. Chen
Institute of Biological Chemistry, Academia Sinica, Taipei, 115, Taiwan

R.-H. Chen, C.P.-K. Lai
Genome and Systems Biology Degree Program, National Taiwan University, Taipei, 10617 Taiwan;

H.-C. Huang, Y.-C. Sung, H. T. Hsieh, K.-W. Huang, Y. Chen

Institute of Biomedical Engineering and Frontier Research Center on Fundamental and Applied Sciences of Matters, National Tsing Hua University, Hsinchu, 30013 Taiwan;

H.-C. Huang, Y.-C. Sung
Department of Chemical Engineering, National Tsing Hua University, Hsinchu, 30013 Taiwan;

Keywords: extracellular vesicles, exosomes, microvesicles, organotropism, biodistribution, breast cancer

Extracellular vesicles (EVs) are released by cells to mediate intercellular communication under pathological and physiological conditions. While small EVs (sEVs; <100–200 nm, exosomes) are intensely investigated, the properties and functions of medium and large EVs (big EVs [bEVs]; >200 nm, microvesicles) are less well explored. Here, we identify bEVs and sEVs as distinct EV populations, and determine that bEVs are released in a greater bEV:sEV ratio in the aggressive human triple-negative breast cancer (TNBC) subtype. PalmGRET, bioluminescence resonance energy transfer (BRET)-based EV reporter, reveals dose-dependent EV biodistribution at non-lethal and physiological EV dosages, as compared to lipophilic fluorescent dyes. Remarkably, the bEVs and sEVs exhibit unique biodistribution profiles, yet individually promote *in vivo* tumor growth in a syngeneic immunocompetent TNBC breast tumor murine model. The bEVs and sEVs share mass spectrometry (MS)-identified tumor progression-associated EV surface membrane proteins (tpEVSurfMEMs), which include SLC29A1, CD9 and CD44. tpEVSurfMEM depletion attenuates EV lung organotropism, alters biodistribution, and reduces protumorigenic potential. This study identifies distinct *in vivo* property and function of bEVs and sEVs in breast cancer, which suggest the significant role of bEVs in diseases, diagnostic and therapeutic applications.

1. Introduction

Extracellular vesicles (EVs) are nanovesicles with a lipid bilayer released by cells to mediate cell–cell communication.[1] Small EVs (sEVs) are <100–200-nm wide, whereas medium or large EVs (big EVs [bEVs]) are >200-nm wide.[2] We termed the bEVs and sEVs as such as their subcellular origins have not been identified, unlike microvesicles and exosomes.[3] Cells also release non-membranous nanoparticles (<50 nm) (exomeres[4] and supermeres[5]) with distinct cargo signatures. Moreover, aggressive cancers release large

oncosomes (1–10 μm) that contain oncoproteins.[6] Since EVs were discovered, most EV studies gravitated towards sEVs and their roles under (patho)physiological conditions.[7] Larger EVs (microvesicles, ectosomes, oncosomes) have been explored but generally without a direct comparison to sEVs.[8] Whereas sEVs have a higher surface-to-volume ratio, bEVs have greater cytosolic volume[9]. Therefore, sEVs and bEVs theoretically demonstrate significant surface presentation and bioactive cargo packaging capability, respectively, to facilitate intercellular communication.

Breast cancer is a highly heterogeneous disease accompanied by a diverse set of clinical characteristics and molecular subtypes.[10] Among the breast cancer subtypes, triple-negative breast cancers (TNBC) lacking estrogen receptor (ER), progesterone receptor (PR), and human epidermal growth factor receptor 2 (HER2) exhibits the worst prognosis, followed by the HER2+, luminal B, and luminal A subtypes.[11] Cancer EVs and the delivered bioactive cargos are important in cancer progression, including tumor growth, angiogenesis, and metastasis.[12] However, whereas most breast cancer EV studies focused on sEVs, fewer investigations methodically explored bEVs in breast cancers and compared the in vivo properties and functions. Moreover, whether the breast cancer subtypes release a differential abundance of specific EV subtypes (bEVs and sEVs) remains largely unexplored.

Tracking EVs in vivo remains difficult due to their size, where EVs typically require labeling for subsequent detection, especially in vivo.[13] EV surface reporters function by labeling the membrane, which rely on EV surface properties to yield optimal labeling, coverage, and signal intensity.[14] Lipophilic dyes (PKH26, DiD, DiR) bind and insert into the lipid bilayer[14a, 15]; while dye-based labeling typically takes a short time to perform, the dyes form nanomicelles to yield false positive signals.[14a, 16] Furthermore, PKH26 and DiR, initially utilized for cell tracking, have an in vivo half-life of 5 to >100 days[17], which may not reflect the true spatiotemporal property of the labeled EVs. In parallel, high-dose labeled EVs (~50–100 μg) are commonly applied in mouse models[14a, 15, 18], which is unlikely to correspond to a physiologically relevant EV dosage.[19] To circumvent these potential caveats, we developed a BRET (bioluminescence resonance energy transfer)-based EV reporter (PalmGRET) to enable multi-resolution imaging and sensitive biodistribution analysis of EVs.[14b]

As we and others have reported, surface membrane proteins can dictate EV *in vivo* dynamics.[14b, 20] Specifically, proteins expressed on the EV surface (tetraspanins, galectins, integrins) enable EVs to interact with membrane proteins on specific recipient cells via a ligand–receptor mechanism for subsequent bioactive cargo entry and delivery.[20a, 21] Both bEVs and sEVs are found to express surface membrane proteins that correspond to their cells of

origin[22]. However, the degree of expression of these membrane proteins in both bEV and sEVs and how it could affect their biodistribution remains largely uncharted, and thus warrant detailed explorations.

In the present study, we examined the bEV and sEV release index in different breast cancer subtypes, and systematically compared EV labeling modalities, dosages, and lethality. We subsequently identified innate biodistribution, organotropic tumor progression-associated EV surface membrane proteins (tpEVSurfMEMs), and individual capacities of TNBC-derived bEVs and sEVs to induce tumorigenesis in vivo. These findings have important implications for bEV- and sEV-mediated cell-cell communication in disease and therapy.

2. Results

2.1. TNBC cells release more bEVs per and sEVs than normal cells. We isolated bEVs and sEVs from human TNBC, HER2+, and ER/PR luminal breast cancer cell lines using differential centrifugation and compared them to EVs from human mammary M10 epithelial cells (**Figure 1a, b**). Nanoparticle tracking analysis (NTA) revealed that the TNBC (MDAMB231, Hs578T, BT549) and ER/PR (MCF7) breast cancer cells released comparable amounts of bEVs and sEVs per cell, whereas HER2+ (SKBR3) breast cancer and M10 epithelial cells released significantly fewer bEVs than sEVs per cell (**Figure 1c, left**). Upon normalization with sEVs, all human TNBC and ER/PR breast cancer cells released higher amounts of bEVs compared to the M10 epithelial cells (**Figure 1c, right**).

The high bEV:sEV ratio of the aggressive TNBC cells suggested that while sEVs enhanced carcinogenesis[23], bEVs may also be important during tumor progression via circulation and distribution *in vivo*. To investigate TNBC-secreted bEVs and sEVs, we used murine TNBC-resembling 4T1 cancer cells as a syngeneic, immunocompetent breast tumor model. Similar to human TNBC cells, the 4T1-derived bEVs (269.27 ± 11.0 nm) demonstrated significantly larger particle sizes than the sEVs (221.67 ± 7.6 nm) (**Figure 1d**), which indicated that 4T1 cells are an ideal donor of TNBC-derived bEVs and sEVs.

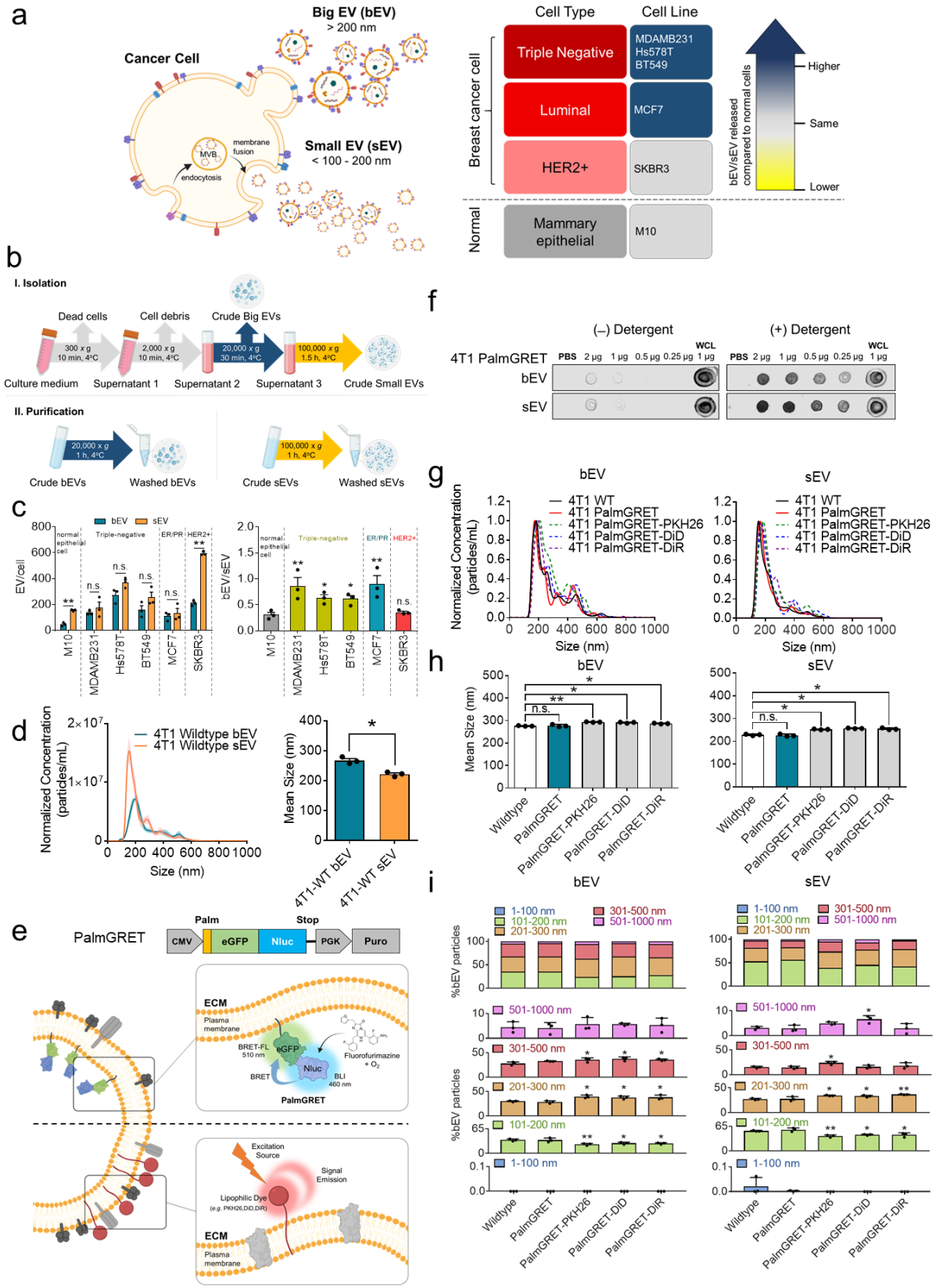

Figure 1. Breast cancers release more bEVs per sEVs than normal cells. a, Diagram showing cancer cell release of bEVs and sEVs. The highly aggressive TNBC and ER/PR breast cancer cells released more bEVs and sEVs as compared to normal cells. **b,** Schematic for bEV

and sEV isolation using differential centrifugation. Conditioned medium (CM) collected from the breast cancer and normal cells underwent differential ultracentrifugation at 20,000 ×*g* and 100,000 ×*g* to isolate bEVs and sEVs, respectively, followed by phosphate-buffered saline (PBS) wash. **c,** NTA of bEVs and sEVs isolated from human breast cancers and normal epithelial cells. Human TNBC (MDAMB231, Hs578T, BT549) and ER/PR (MCF7) breast cancer cells released comparable amounts of bEVs and sEVs per cell while human HER2+ SKBR3 breast cancer and M10 normal human epithelial cells released significantly lower amounts of bEVs than sEVs per cell (left; determined from three independent experiments). Human TNBC and ER/PR breast cancer cells released significantly higher bEV-to-sEV ratios as compared to HER2+ cells and normal human epithelial cells (right). **d,** NTA of 4T1-bEVs and -sEVs demonstrating distinct size distributions (left; representative data of three independent experiments) and mean sizes (right; determined from three independent experiments). **e,** Schematic of inner EV membrane labeling using PalmGRET (top) and outer EV membrane labeling using lipophilic fluorescent dyes (bottom). PalmGRET labels the EV lipid bilayer inner leaflet via its palmitoylation moiety to enable multi-resolution imaging and sensitive biodistribution analysis of EVs.[14b] By contrast, lipophilic dyes label EVs by insertion into the lipid bilayer. **f,** Dot blot analysis showing that PalmGRET labeled the inner membrane of bEVs and sEVs. If PalmGRET is located in the inner membranes, antibodies would be unable to access the reporter protein unless the EV membrane is disrupted. Conversely, the addition of Tween 20 disrupts the EV membrane to allow access to antibodies to bind the PalmGRET. A strong PalmGRET signal was detected only in the presence of 0.1% (v/v) Tween 20 detergent in a dose-dependent manner, which indicated inner EV membrane-specific labeling of bEVs and sEVs derived from stable 4T1-PalmGRET cells. The positive control was whole cell lysates (WCL). **g–i,** NTA of PalmGRET- and dye-labeled 4T1-EVs. Size distribution **(g)** and mean size **(h)** of bEVs and sEVs labeled with PalmGRET or co-labeled with PKH26, DiD, and DiR are shown. Analysis of particle size composition of the bEVs and sEVs **(i)** showed that PalmGRET did not change the size distribution in all size divisions as compared to the WT EV controls. The 101–200-nm particles were decreased while the 201–300-nm and 301–500-nm particles were increased among the lipophilic dye-labelled bEVs. Similarly, the 101–200-nm particles were decreased and 201–300-nm particles were increased among the lipophilic dye-labelled sEVs. The WT-bEVs predominantly comprised 101–200-nm (35.29%), 201–300-nm (29.69%), and 301–500-nm particles (27.87%) and fewer 501–1000-nm particles (4.49%) (left). By contrast, the WT-sEVs mainly consisted of 101–200-nm (52.82%) and 201–300-nm particles (27.01%) and fewer 301–500-nm (15.04%) and 501–1000-nm particles (3.10%)

(right). These results indicated that the bEVs and sEVs were comprised of distinct-size EV subpopulations. Data are from three independent experiments. n.s., $p > 0.05$; *$p < 0.05$; **$p < 0.01$ with 1-way ANOVA followed by Dunnett's post hoc test vs. the control.

2.2. Comparison of size and detection limit between PalmGRET- and dye-labeled bEVs and sEVs. To accurately track EV spatiotemporal properties *in vivo*, it is critical that the labeling technique (**Figure 1e)** does not alter the EV native physicochemical characteristics. 4T1-PalmGRET-EVs underwent dot blot analysis and strong PalmGRET protein signals were detected only in the presence of Tween 20, and vice versa, thereby validating the EV inner membrane specificity of PalmGRET for labeling bEV and sEVs. (**Figure 1f**).

NTA of EVs isolated from wild-type 4T1 (4T1-WT, control) and stable 4T1-PalmGRET cells was performed to investigate whether PalmGRET or the lipophilic dyes would alter EV size (**Figure 1g**). Concurrently, we examined PKH26-, DiD-, or DiR -labeled 4T1-PalmGRET-EVs. The PalmGRET-bEV and -sEVs exhibited similar size distribution patterns when compared to the control. By contrast, the PKH26-, DiD-, and DiR-labeled bEVs and sEVs demonstrated increased size distributions. Similarly, the mean size of the WT- and PalmGRET-EVs did not vary, whereas the dye-labeled bEVs and sEVs exhibited significantly larger mean sizes (**Figure 1h**).

We compared the size distributions between the WT-, PalmGRET-, and dye-labeled EVs (**Figure 1i**). The PalmGRET-bEVs and -sEVs did not vary significantly compared to the WT-EVs, which suggested that PalmGRET labeling retained the original particle size heterogeneity for both bEVs and sEVs. Conversely, the lipophilic dye labeling increased EV sizes at specific size ranges, thereby altering the overall EV size distribution patterns.

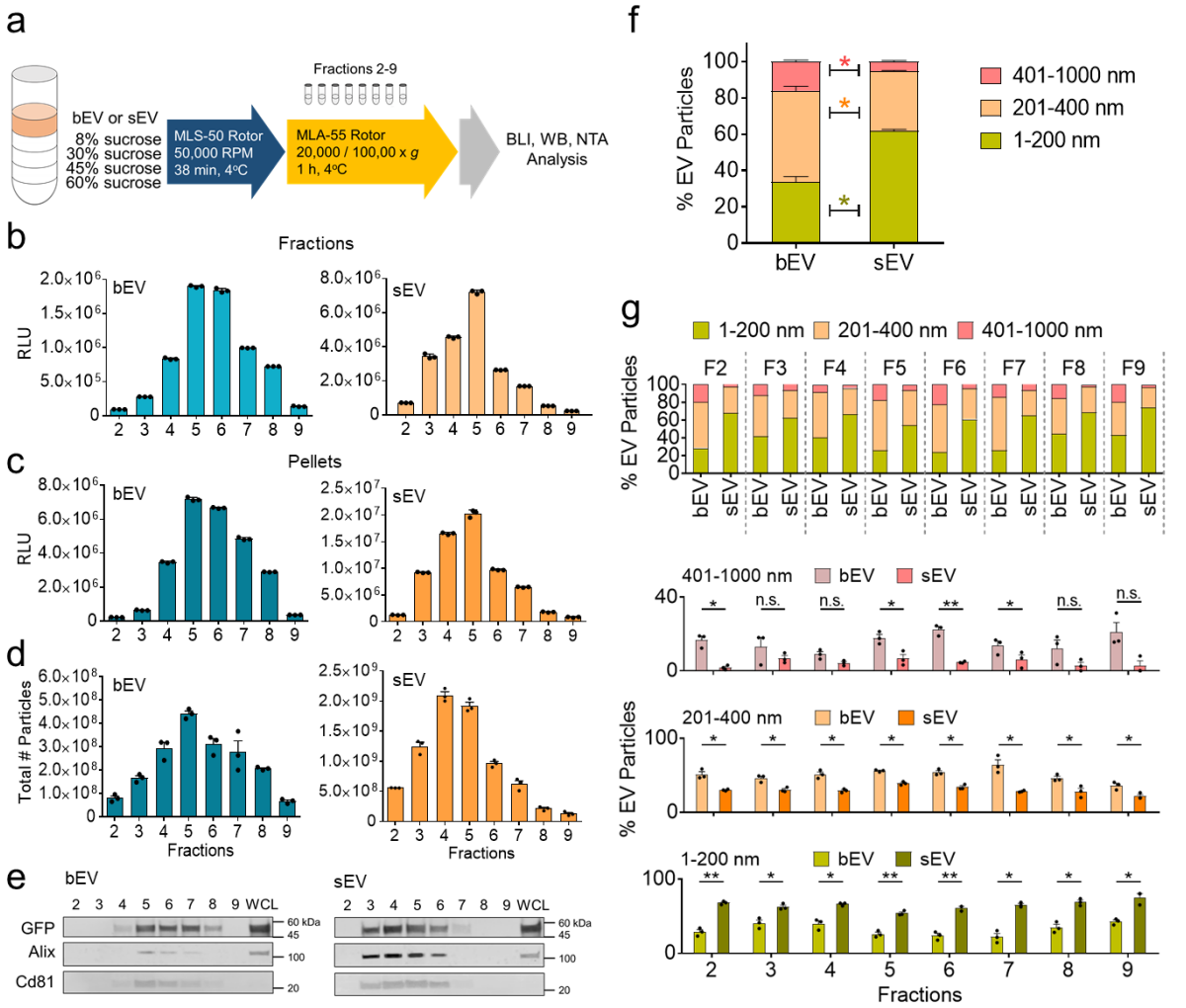

Figure 2. bEVs and sEVs differ in size composition and density. a, Flowchart of sucrose gradient fractionation of 4T1-PalmGRET-bEVs and -sEVs. **b, c,** Nluc assay of the EVs following fractionation **(b)** and fraction pelleting **(c)**. **d,** NTA of pelleted sucrose gradient fractions. **e,** Western blotting of bEV (left) and sEV (right) proteins from the pelleted fractions revealing that PalmGRET (49 kDa) coincided with the Alix (96 kDa) and CD81 (20 kDa) EV markers. The positive control was WCL. **f,** Total particle size composition analysis (fractions 2–9) showing that bEVs were composed of a significantly higher percentage of 201–400-nm particles (bEV: 50.47% vs. sEV: 32.85%) and 401–1000-nm particles (bEV: 16.03% vs. sEV: 5.42%), whereas sEVs were primarily comprised of 101–200-nm particles (bEV: 33.50% vs. sEV: 61.73%). **g,** Particle analysis of sucrose gradient fractions demonstrating that bEVs and sEVs had significantly different size distribution in the 101–200-nm (all fractions), 201–400-nm (all fractions), and 401–1000-nm (fractions 2, 5–7) size ranges. n.s., $p > 0.05$; *$p < 0.05$; **$p < 0.01$ with 2-tailed Student's *t*-test.

2.3. bEVs and sEVs exhibit differing composition sizes and densities. To determine detailed bEV and sEV size composition, freshly isolated EVs underwent sucrose density gradient fractionation followed by biophysical characterizations (**Figure 2a**). Bioluminescent assay (BLI) and NTA revealed that bEVs and sEVs were enriched in overlapping but different sucrose density fractions (**Figure 2b–d**). The BLI signals detected pre- (**Figure 2b**) and post-fraction pelleting (**Figure 2c**) positively corroborated with the particle concentration determined by NTA (**Figure 2d**). Whereas bEVs were primarily enriched in fractions 4–8, sEVs were mainly present in fractions 3–6. In accordance with these results, western blotting of the pelleted EVs demonstrated that PalmGRET coincided with EV markers (CD81 and Alix [ALG-2-interacting protein X]) in the bEV and sEV enriched fractions (**Figure 2e**). Alix was more enriched in the sEV than bEV enriched fractions. The total particle composition analysis revealed that the bEVs were composed of a higher percentage of 201–400- and 401–1000-nm particles as compared to the sEVs (**Figure 2f**). Additional characterization to compare the particle composition profiles in each density fraction demonstrated that the bEVs and sEVs had significantly different percent particle size distributions in the 101–200-, 201–400-, and 401–1000-nm ranges (**Figure 2g**).

These results demonstrated that the bEVs and sEVs consisted of particles with lower and higher densities, respectively. Furthermore, while the density fractionation demonstrated that the bEVs and sEVs shared overlapping densities, the fractions comprised significantly different particle size composition profiles.

2.4. bEVs have a greater surface area per particle than sEVs. Fluorofurimazine (FFz) is a modified version of furimazine (Fz) with improved water solubility and hence greater reactivity with Nluc luciferase (enhanced signal).[24] We tested the applicability of FFz, and demonstrated that FFz could be applied to enhance BLI and BRET-FL (fluorescence) activities of PalmGRET-labeled bEVs and sEVs (**Figure S1, S2**).

We examined the BLI properties of PalmGRET-bEVs and -sEVs by measuring BLI and BRET-FL activities supplemented with FFz over time. Following normalization to EV particles, Nluc (**Figure 3a**) and BRET-FL (**Figure 3b**) demonstrated that bEVs exhibited higher signal intensity per particle when compared to the sEVs. Contrastingly, Nluc (**Figure 3c**) and BRET-FL (**Figure 3d**) per protein were higher in the sEVs than bEVs. The half-life of the signals and BRET ratios (**Figure 3e**) were comparable under both normalization settings, which indicated that PalmGRET functioned similarly in the labeled bEVs and sEVs. The protein concentration assay indicated no difference in the total protein amount between the bEVs and sEVs from each EV isolation batch (**Figure 3f**). Furthermore, the sEVs exhibited a higher RLU (relative light

units) per protein than the bEVs (**Figure 3g**) while there were more sEV particles than bEVs per protein (**Figure 3h**). The bEVs demonstrated a higher RLU × ng/particle (**Figure 3i**). The results indicated that bEVs are distinct EV population with a greater surface area per particle than sEVs.

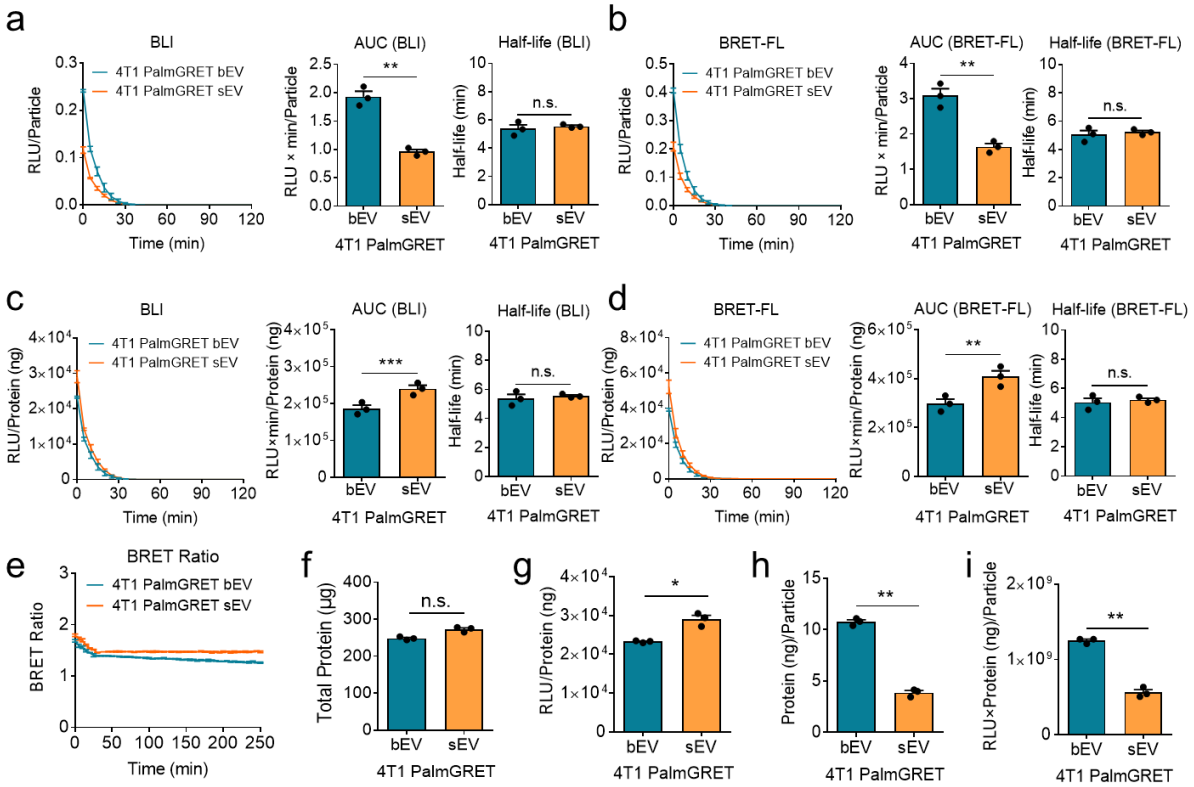

Figure 3. PalmGRET demonstrates that bEVs contain more protein per particle than sEVs. a, b, Following normalization to EV particles, Nluc **(a)** and BRET-FL **(b)** demonstrated that bEVs had higher signal intensity (area under the curve [AUC]) per particle when compared to sEVs. **c, d,** Following normalization to EV protein amount, Nluc **(c)** and BRET-FL **(d)** revealed that sEVs had higher RLU per protein (ng). **e,** Half-life of the signals and BRET ratio were comparable under both normalization settings, which indicated that the PalmGRET reporter functioned similarly in bEVs and sEVs. **f,** Protein concentration assay indicated no significant difference in total protein amount between bEVs and sEVs from each EV isolation batch. **g,** sEVs exhibited higher RLU per protein (ng) than bEVs. **h,** Bar graphs showing significantly more protein (ng) per bEV particle than sEVs. **i,** Bar graphs indicating bEVs exhibited higher RLU × ng/particle.

2.5. PalmGRET labeling exhibits a high dynamic range (HDR), and enables sensitive EV biodistribution analysis at non-lethal low dosages *in vivo.* We compared the detection limits and linearity between the PalmGRET and DiR signals of 4T1-PalmGRET-DiR-bEVs and -sEVs (**Figure 4a, b**). PalmGRET signals were detected with a high correlation to EV protein concentration in bEVs (R^2 = 0.9788) and sEVs (R^2 = 0.9720) (**Figure 4a**). Contrastingly, DiR signals demonstrated a lower correlation in bEVs (R^2 = 0.9318) and sEVs (R^2 = 0.8003) and were barely at concentrations < 125 or 0–1000 ng, respectively (**Figure 4b**). These findings indicated that PalmGRET exhibited HDR and linearity even at low EV protein concentrations as compared to DiR.

To investigate the possible effect of dosage and DiR labeling on EV biodistribution, we administered 10, 25, 50, or 100 µg 4T1-PalmGRET-DiR-bEVs or -sEVs intravenously (IV) into immunocompetent BALB/c mice (**Figure 4c**). Unexpectedly, a high lethality rate was observed in both the 50 µg and 100 µg bEV and sEV groups, with no surviving animals at 24 h (**Figure 4d**). By contrast, there were minimal or no deaths in the 10 µg and 25 µg bEV and sEV groups at 24 h post-injection. This result indicated that ≥50 µg labeled 4T1 EVs presented a high lethality risk to the mice.

We subsequently performed biodistribution analyses based on BRET-FL (PalmGRET) and FL (DiR) signals of the 10 µg and 25 µg bEV and sEV groups (**Figure 4e**). PalmGRET signal revealed that 4T1-bEVs and -sEVs primarily targeted the lung, liver, and spleen (sEV only) at a low dose. Notably, the temporal change in bEV biodistribution was not as prominent as that of sEVs in the 10 µg groups, which suggested that sEVs are more readily trafficked to the liver from other major organs over time, which could only be observed with low-dose EV (10 µg). The DiR signal intensity was weak and with a high background in the 10 µg and 25 µg groups (**Figure S3, Table S1, S2**). This rendered DiR signals mostly detectable in a large major organ (the liver) but not in the other smaller major organs.

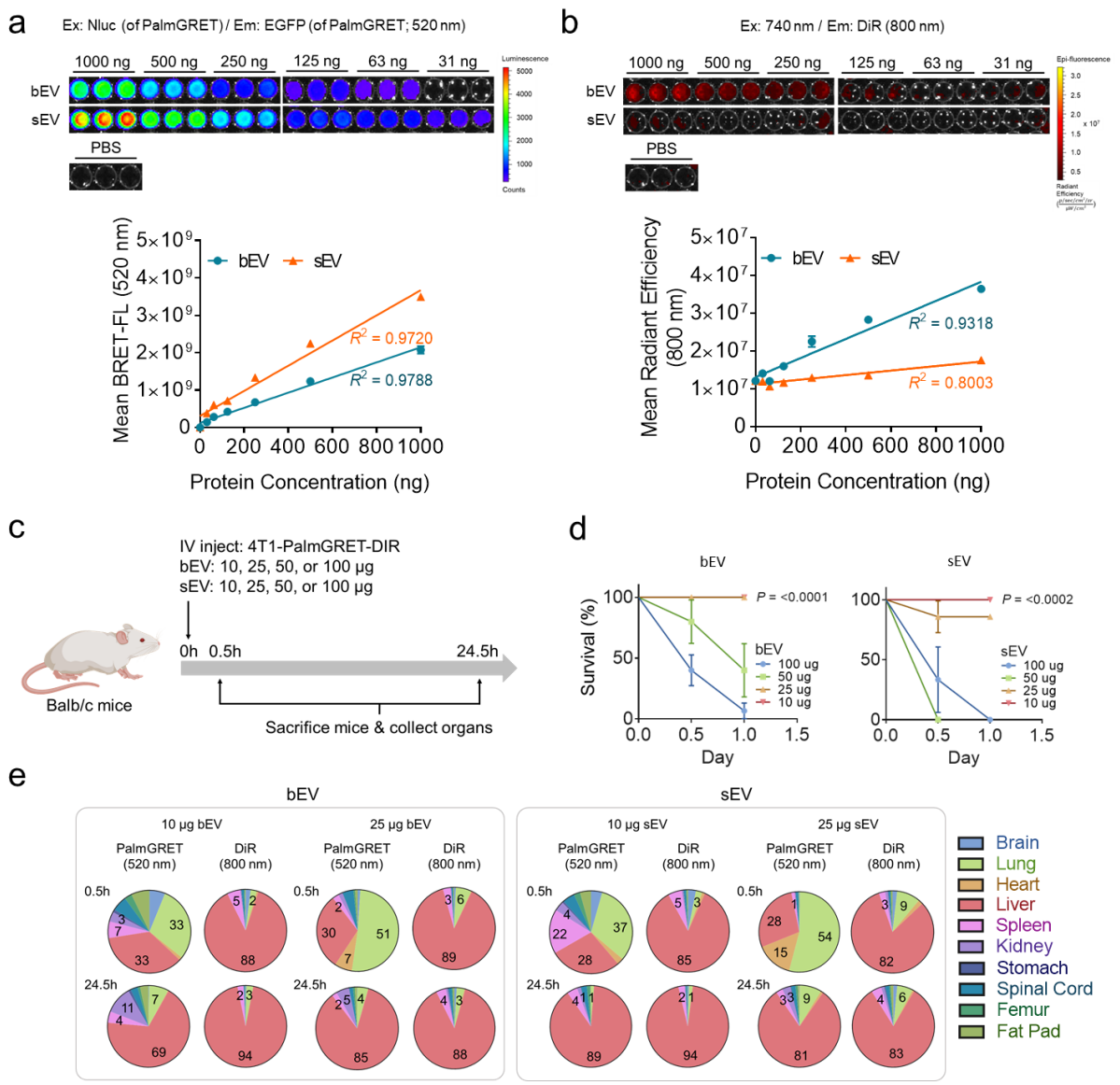

Figure 4. EV PalmGRET labeling enables sensitive EV biodistribution analysis at non-lethal low dosages *in vivo*. a, BRET-based EGFP signal of PalmGRET-DiR 4T1-EVs (top) demonstrating a HDR (10^9) of PalmGRET BRET-FL signals (bottom). **b,** External excitation-based DiR signal of PalmGRET-DiR 4T1-EVs (top) showing a low dynamic range of DiR signals (~10^7; bottom). n.s., $p > 0.05$; *$p < 0.05$; **$p < 0.01$, ***$p < 0.001$ with 2-tailed Student's *t*-test. **c,** Pharmacokinetics study of 10–100 µg PalmGRET-DiR 4T1-EVs in mice. **d,** Survival rate of IV-injected mice. Only 10 µg (bEVs and sEVs) and 25 µg (bEVs only) yielded full survival among the mice (4 out of 4 per group). **e,** Differential biodistribution pattern between PalmGRET and DiR signals of IV-injected 4T1-PalmGRET-DiR EVs over time. In the 25 µg groups, PalmGRET signals of both bEV and sEV exhibited the highest initial (0.5 h) distribution to the lungs followed by the liver. At 24.5 h, both bEVs and sEVs were decreased in the lungs and predominantly accumulated in the liver. In the 10 µg groups, bEVs

demonstrated the highest initial (0.5 h) distribution in the lungs and liver, whereas sEVs were detected primarily in the lungs, liver, and spleen. At 24.5 h, both bEVs and sEVs were decreased in the lungs and predominantly accumulated in the liver. Oppositely, the bEV and sEV DiR signals in both the 10 μg and 25 μg groups demonstrated high distribution to the liver at 0.5 h and 24.5 h, revealing a distinct EV biodistribution pattern compared to that of PalmGRET (**Supplementary Table 3**).

2.6. Reduced tpEVSurfMEM expression attenuates lung tropism and alters bEV and sEV biodistribution. To investigate the proteins that may contribute to 4T1 EV lung tropism, 4T1-bEV and -sEV protein were screened based on their prior association with breast cancer tumorigenesis and metastasis to identify three EV lung tropism-related tpEVSurfMEMs: solute carrier family 29 member 1 (Slc29a1), tetraspanin Cd9, and cell surface glycoprotein Cd44 (**Figure 5a, b, Figure S4**).

We next explored the roles of the identified tpEVSurfMEM candidates in directing bEV and sEV innate organotropism *in vivo* using 4T1-PalmGRET. We generated stable cell lines to knockdown (KD) the candidates of the bEVs and sEVs by transducing 4T1-PalmGRET cells using lentivirus encoding short hairpin RNAs (shRNAs) targeting a null sequence (Scramble) or the tpEVSurfMEMs **(Figure 5c, Figure S5, Table S3**). shCd44- and shSlc29a1-EVs demonstrated significantly reduced distribution to the lungs at 0.5 h post-injection as compared to the Scramble controls, which suggested a role of Cd44 and Slc29a1 in the immediate direction of bEVs and sEVs to the lungs (**Figure 5d, e, Figure S6, Table S4)**. By contrast, the shCd9-EVs demonstrated reduced lung distribution only at 72.5 h, which indicated that Cd9 may also facilitate EV lung tropism but via a slower mode of action than Cd44 and Slc29a1. Significantly reduced RLU intensities of shCd9-, shCd44-, and shSlc29a1-bEVs and shCd9-sEVs were detected in the liver at 0.5 h (**Figure 5f**). Significantly reduced RLU intensities of shCd9-, shCd44-, and shSlc29a1-sEVs were detected in the spleen at 0.5 h and 72.5 h, this trend was not observed in the bEVs, which suggested that bEVs and sEVs may follow different routes toward splenic uptake. The shCd44-bEV and -sEV signals were higher in the blood at 72.5 h (**Figure 5f)**, which suggested that the reduced uptake by the major organs freed and subsequently increased circulating EV concentrations in the blood. Overall, the results demonstrated that KD expression of bEV and sEV shared tpEVSurfMEMs reduced lung tropism and elevated circulating EV levels in the blood.

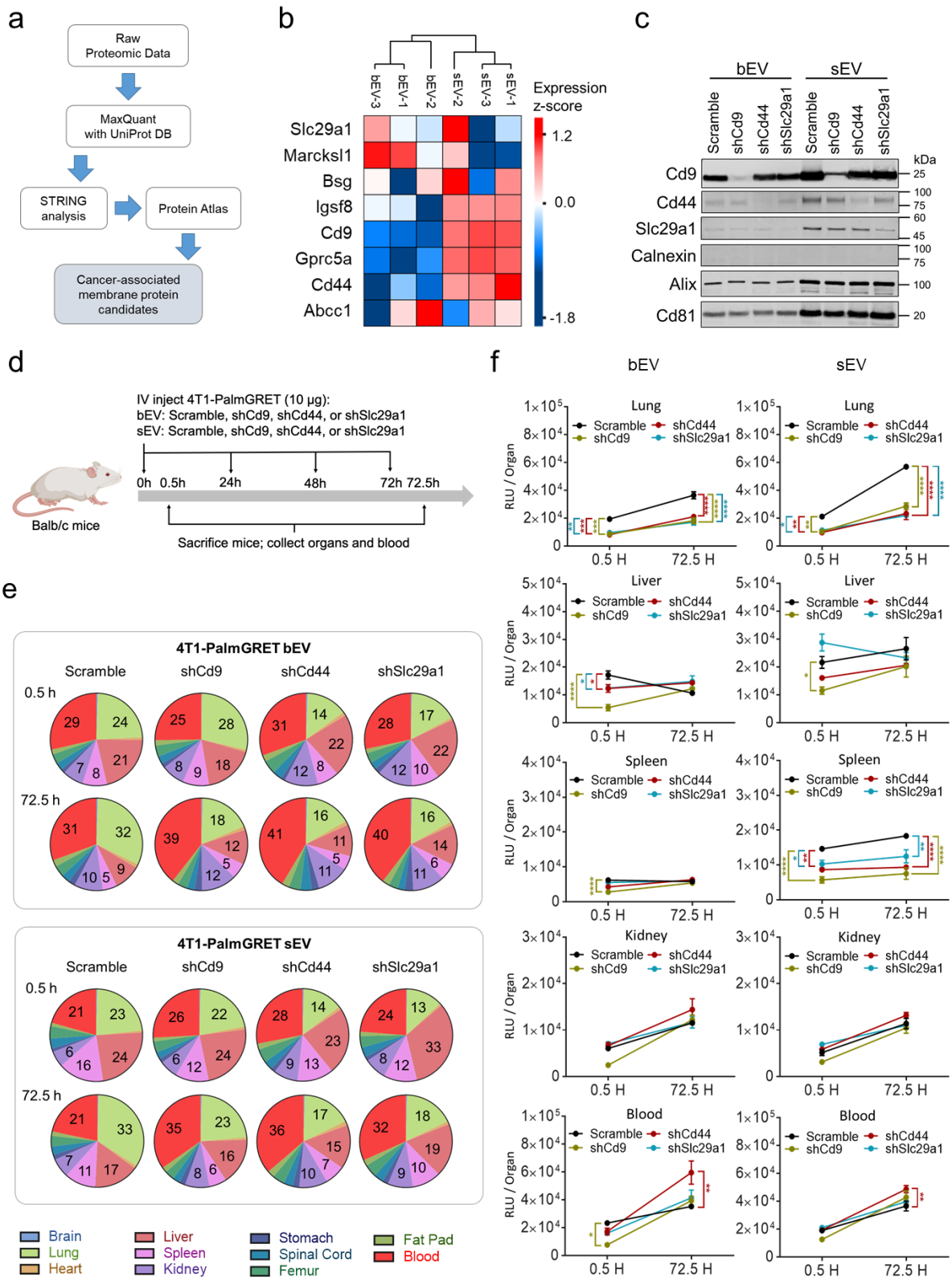

Figure 5. Reduced tpEVSurfMEM expression attenuates lung tropism and alters breast cancer bEV and sEV biodistribution. a, Flowchart of proteomics analysis to identify cancer-associated EV membrane protein candidates. 4T1-bEV and -sEV protein samples underwent liquid chromatography–tandem mass spectrometry (LC-MS/MS) analysis. The relative protein abundance in each sample group was determined using label-free quantification. Three

biologically independent samples of bEVs and sEVs were analyzed using LC-MS/MS and MaxQuant, followed by manual STRING and the Human Protein Atlas database annotations to screen for cancer-associated membrane proteins. **b,** Heatmap illustrating the relative abundance of membrane and membrane-associated proteins identified in 4T1-PalmGRET-bEVs and -sEVs with prior cancer relation annotated in UniProt, i.e., tpEVSurfMEMs. **c)** Western blot demonstrating KD of selected candidates in bEVs and sEVs. 4T1-PalmGRET cells were stably transduced with lentivirus encoding shRNA targeting the null sequence (Scramble) or individual tpEVSurfMEMs followed by EV isolation and western blotting analysis: CD9 (25 kDa); CD44 (85 kDa), and SLC29A1 (55 kDa). The cell marker (negative EV control) was calnexin (85 kDa). Alix (96 kDa) and CD81 (26 kDa) were immunoprobed as EV markers. **d,** Schematic for the redirection of EV organotropism where 4T1 BALB/c mice were IV-injected with EVs (10 µg) at 0, 24, 48, and 72 h through the tail vein, and the organs were collected for biodistribution analysis at 0.5 h and 72.5 h. **e,** EV biodistribution percentage pie chart demonstrating reduced lung tropism and altered distribution at organ system level of shCd9-, shCd44-, and shSlc29a1-4T1-PalmGRET-sEVs and -bEVs when compared to the Scramble controls over 3-day EV treatment. shCd44- and shSlc29a1-EV lung distribution was strongly decreased beginning at 0.5 h, which persisted to 72.5 h. shCd9-EVs demonstrated reduced lung distribution only at 72.5 h. The EV distribution percentage for each organ at different time points were calculated as the mean organ RLU per mean RLU of all organs. $N = 3$ mice per group with technical triplicates for each sample. **f)** Total EV signals of shCd9-, shCd44-, and Slc29a1-4T1-PalmGRET-sEV and bEV distribution in the lung, liver, kidney, spleen, and blood compared to that of the Scramble controls. Data are the mean ± SEM. $*p < 0.05$; $**p < 0.01$ with 2-way ANOVA followed by Dunnett's post hoc test vs. Scramble controls.

2.7. bEVs and sEVs individually promote breast cancer tumor growth. To mimic and investigate if constant exposure to cancer bEVs and sEVs in the circulation had a protumorigenic function, syngeneic immunocompetent 4T1 tumor-bearing mice received IV 10 µg 4T1-PalmGRET-Scramble- and -shCd44-bEVs and -sEVs, or PBS (control) three times weekly (**Figure 6a**). Scramble-bEV and -sEV groups yielded significantly higher tumor weights and volume, as well as lower body weights as compared to the control, which suggested that bEVs and sEVs individually induced a protumorigenic effect (**Figure 6b, c**). Moreover, the shCd44-bEV and -sEV groups demonstrated similar tumor weights and volumes as compared to the control, which indicated that depleting Cd44 in the EVs attenuated the

protumorigenic potential of 4T1-EVs (**Figure 6b**). Biodistribution analysis of the EVs in the tumor-bearing mice revealed distinct distribution profiles between the Scramble- and shCd44-EVs, where shCd44-sEVs and -bEVs significantly reduced lung distribution and increased circulation in the blood (**Figure 6d, Figure S7, Table S5**). Furthermore, both shCd44-bEVs and -sEVs exhibited significantly decreased distributions to the tumor as compared to the Scramble controls (**Figure 6e**). We validated bEV and sEV distribution in the lung, spleen, and tumors via super-resolution microscopy (**Figure 6f, g, Figure S8a**). Z-stack imaging demonstrated intracellular bEV and sEV uptake in the spleen, lung, and tumors of mice treated with 4T1-PalmGRET-Scramble- or shCd44-bEVs or -sEVs (**Figure S8b**). Altogether, our results reveal that Cd44 is pivotal in promoting tumor growth individually via either bEVs or sEVs and that reduced Cd44 expression redirected organotropism and subsequent change in biodistribution at organ system level.

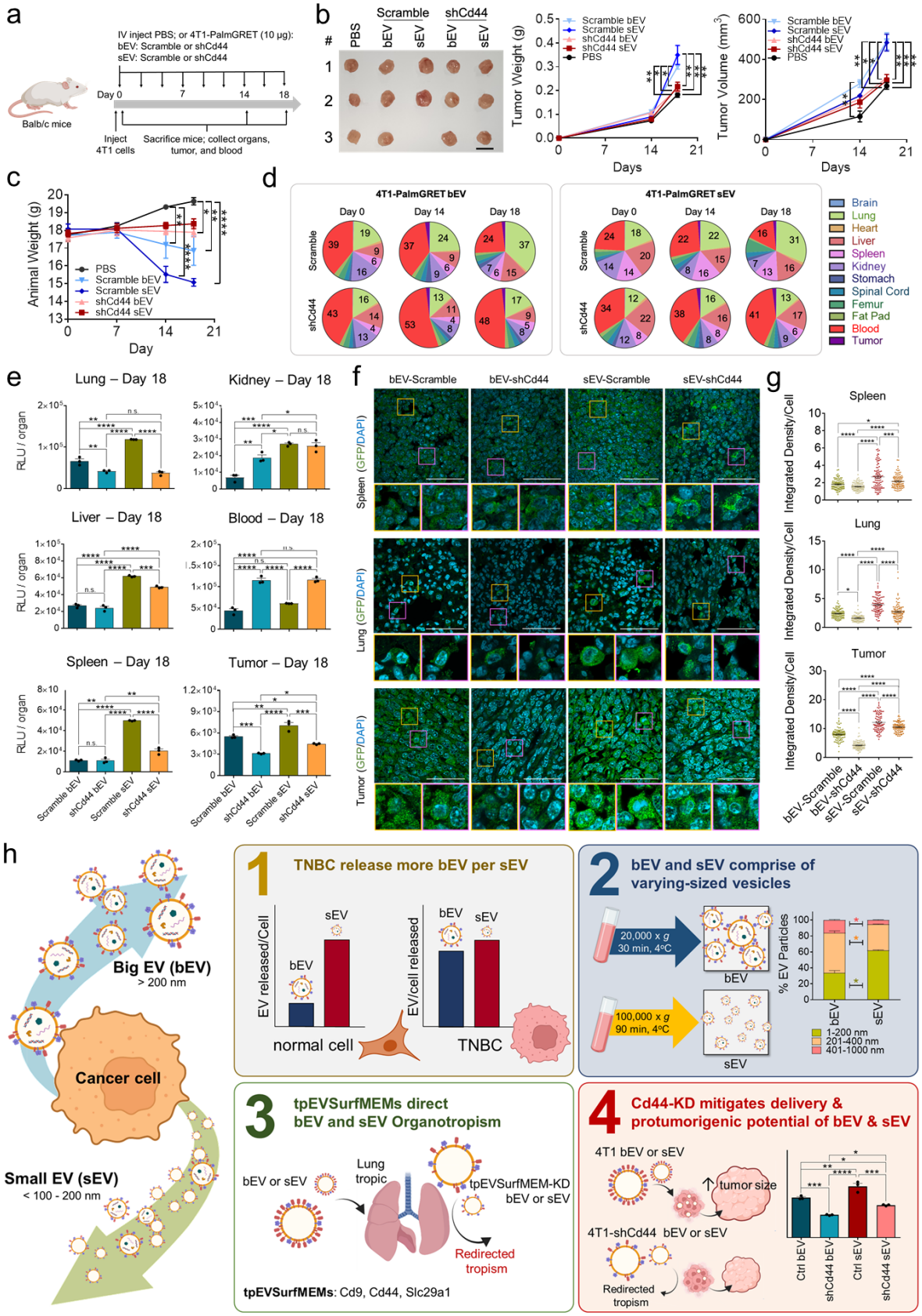

Figure 6. Lung tropic cancer-derived EVs promote breast cancer tumor growth; Depleting CD44 in cancer bEVs and sEVs reduces EV cellular uptake in the spleen, lung, and tumor. a, Schematic of tracking biodistribution and tumorigenic effect of IV lung tropic

4T1-EVs in the syngeneic 4T1-BALB/c orthotopic breast cancer model. BALB/c mice were subcutaneously injected with 5×10^4 4T1 cells in the fat pad. The mice received PBS, Scramble bEV/sEV (10 μg), or shCd44 bEV/sEV (10 μg) thrice per week for 18 days. The blood and organs were harvested at day 0, 14, and 18 for biodistribution analysis. **b,** Isolated orthotopic 4T1 tumors (left) on day 18. Bar, 10 mm. Tumor weight (middle) and tumor volume (right) at day 14 and 18. $N = 3$ per group. **c,** Animal weight from day 0 to 18 post-4T1 implantation and EV administration. $N = 4$ mice per group. n.s., $p > 0.05$; $*p < 0.05$; $**p < 0.01$; $***p < 0.001$; $****p < 0.0001$ with 1-way ANOVA followed by multiple group comparisons. **d,** Pie charts showing significantly reduced lung distribution and increased circulation in the blood of shCd44-sEVs and -bEVs in the tumor-bearing mice. At day 14 and 18 post-EV treatment, fewer shCd44-bEVs and -sEVs were distributed to the lungs as compared to the Scramble controls, corroborating our findings that Cd44 depletion in EVs attenuated lung tropism (**Fig. 5e**). In the spleen, Scramble-sEV biodistribution was higher than that of the Scramble-bEVs. While there was no difference between shCd44-bEV and Scramble-bEV biodistribution in the spleen, significantly reduced shCd44-sEV levels were detected in the spleen compared to Scramble-sEVs, which suggested that Cd44 depletion in the tumor-bearing mice might have reduced the innate delivery of 4T1-sEVs to the spleen. There were higher levels of both shCd44-bEVs and -sEVs in the blood as compared to the Scramble controls, which indicated that the reduced EV uptake by the major organs consequently increased shCd44-EV circulation in the blood. Both shCd44-bEVs and -sEVs exhibited significantly decreased distributions to the tumor as compared to the Scramble controls. The proportions for each organ at different time points were calculated as the mean organ RLU per mean RLU of all organs. $N = 3$ mice per group with technical triplicates. **e,** Bar graphs comparing the Nluc activity among the IV-injected 4T1-PalmGRET-shCd44-bEVs and -sEVs (after 18-day EV treatment) as compared with the Scramble controls are shown. $*p < 0.05$; $**p < 0.01$ 2-tailed Student's *t*-test. **f, g,** Super-resolution imaging **(f)** and quantification of EV signals **(g)** in the spleen, lung, and tumor sections of mice injected with 4T1-PalmGRET-Scramble/shCd44-bEVs or -sEVs. **f,** Representative super-resolution confocal images of the spleen (b), lung (c), and tumor (d) sections collected after 18-day treatment with 4T1-PalmGRET-Scramble or -shCd44-bEVs or -sEVs. Subcellular EV signals were uniformly distributed in the spleen and tumor, while EV distribution in the lungs was sporadic. All tissue section groups were prepared under similar conditions. The nuclei were stained with DAPI and 4T1-PalmGRET was immunoprobed by anti-GFP antibody followed by Alexa Fluor 568-conjugated secondary antibody. Bottom inset of each row depicts the enlarged images of the boxed regions (yellow and purple). Bar, 50 μm.

g, Quantification of EV signals in the tissue sections in (d) demonstrated significantly decreased integrated density per cell in the lung and tumor of mice treated with shCd44-bEVs and -sEVs as compared to the Scramble controls. Only the spleen of shCd44-sEV-treated mice exhibited significantly decreased integrated density per cell as compared to the shCd44-bEV and Scramble control groups. All data are the mean ± SEM. *$p < 0.05$; **$p < 0.01$; ***$p < 0.001$; ****$p < 0.0001$ with 1-way ANOVA followed by multiple group comparisons. **h,** Graphical summary showing that aggressive TNBC released more bEVs per sEVs than normal mammary epithelial cells. Systematic characterization reveals that TNBC-derived bEVs and sEVs exhibited distinctly different particle size compositions and innate *in vivo* biodistribution profiles. Despite these differences, both bEVs and sEVs demonstrated similar degrees of tropism to the tumor and induced protumorigenic effects upon long-term *in vivo* treatment. Both the tropism to tumor and protumorigenic potential of the bEVs and sEVs were remarkably attenuated upon genetic modification of the EV surface membrane (i.e., depletion of CD44 expression).

3. Discussion

bEVs and sEVs theoretically demonstrate significant bioactive cargo packaging capability and surface presentation, respectively[9], to facilitate intercellular communication. Hence, we speculated that both bEVs and sEVs circulate in organisms to exert biological functions. Here, we compared the biophysical properties, biodistribution, and biological effects of bEVs and sEVs from different breast cancer molecular subtypes.

Despite the seemingly overlapping fractions between the bEVs and sEVs, comparison of the particles recovered in each sucrose fraction determined that the bEVs were composed of a significantly lower percentage of 101–200 nm particles and a higher percentage of 201–400-nm and 401–1000-nm particles when compared to the sEVs. By convention, the EV surface area-to-volume ratio increases with the decrease in the EV radii and vice versa. Therefore, sEVs have a much greater surface area per unit volume compared with bEVs.[25] Indeed, PalmGRET demonstrated that the bEVs had higher BL activity per particle when compared to sEVs. Concurrently, the sEVs had higher BL activity per protein (ng) than the bEVs. Altogether, these results suggested that the bEVs and sEVs are different sized EV populations.

Subsequently, we identified PalmGRET as the optimal labeling method for *in vivo* study of bEVs and sEVs that would enable sensitive and accurate EV detection. EVs are labelled with lipophilic dyes initially designed and used to label cells for long-term observation (days to

months), which yield false positive signals (micelle formation) and inaccurate spatiotemporal properties (extended half-life).[13a, 26] Detailed NTA revealed that PKH26, DiD, and DiR labeling but not PalmGRET labeling altered particle size distribution and therefore the mean bEV and sEV sizes, which might have affected their spatiotemporal properties *in vivo* as previously reported for synthetic nanoparticles.[27] Biodistribution analysis showed that DiR affected the normal biodistribution of the labeled EVs over time, possibly with the prolonged half-life and lipophilic property of the dye to be recycled into cellular membranes.[13a, 28] The almost full lethality of high-dose EVs indicated that ≥50 μg is not a physiologically relevant dosage, and warrants attention in future investigations. Whether the lethality is attributed to the EV donor cell type (some cell-derived EVs tend to aggregate more than others; unpublished observation), the dyes, or both is unknown. Accordingly, we used PalmGRET and low-dose EVs (10, 25 μg) in subsequent bEV and sEV experiments.

PalmGRET demonstrated a size-, dose-, and time-dependent EV biodistribution profile. EV size-dependent distribution was observed in the 25 μg set, where more sEVs were trafficked to the heart than bEVs. More sEVs accumulated to the spleen in the 10 μg group, which supported the findings of Wen and colleagues.[29] The bEVs did not accumulate in the spleen as much as the sEVs, which suggested that an EV subtype-dependent mechanism could regulate splenic uptake. Furthermore, at 24 h-post injection, sEV signals were detected predominantly in the liver while bEV signals remained detectable in the liver, kidney, lung, and spleen, which indicated that the organs might process bEVs and sEVs differently. Our findings indicated that bEVs and sEVs are distinct EV populations which can be well circulated with differential biodistribution properties.

EV surface proteins (tetraspanins, galectins, integrins) can dictate EV *in vivo* dynamics via a ligand–receptor mechanism for subsequent bioactive cargo entry and delivery.[14b, 20-21] Here, we identified and subsequently validated the three tpEVSurfMEMs (CD44, CD9, SLC29A1) shared by bEV and sEV in directing their organotropism. As CD44 was overexpressed in invasive breast cancers and metastasis[30], we depleted Cd44 in the bEVs and sEVs and observed a significant decreased tumor delivery and growth while exerting EV population-specific change in the biodistribution pattern. These detailed observations suggested that bEVs and sEVs actively promote breast tumor growth *in vivo* via the circulation and systemic organ and tumor uptake while acting simultaneously under distinct biodistribution patterns. As the TNBC and ER/PR breast cancer cells released both EV subpopulations concurrently, future investigations should elucidate a synergistic (or separate) interplay between bEVs and sEVs.

4. Conclusion

Beyond the general EV perspective, our work provided firm evidence on the equally significant role of bEVs in understanding the systemic importance of EVs *in vivo* (**Figure 6h**). As both bEVs and sEVs interplay during disease progression, it is crucial to elucidate their biodistribution profiles to understand how they might potentially mitigate disease development. Furthermore, this work identified opportunities for future exploratory efforts on therapies that might attenuate breast cancer progression by potentially blocking CD44 in tumor bEVs and sEVs, or selectively detecting and depleting tumor-specific EVs in the circulation.

5. Methods

Cell culture. Murine 4T1 breast cancer cells (gifted by Dr. Yunching Chen, National Tsing Hua University [NTHU], Tsinchu, Taiwan), human mammary epithelial M10 cells, human TNBC MDAMB-231, BT549 (gifted by Dr. Ruey-Hwa Chen, Academia Sinica, Taipei, Taiwan), and Hs578T (Bioresource Collection and Research Center, Hsinchu, Taiwan) cells were maintained in Dulbecco's modified Eagle's medium (DMEM; 4500 mg L^{-1} high glucose, HyClone, South Logan, UT, USA) supplemented with 10% fetal bovine serum (FBS; HyClone), 100 U mL^{-1} penicillin (HyClone), and 100 µg mL^{-1} streptomycin (HyClone). ER/PR (SKBR3) and HER2+ (MCF7) breast cancer cells (gifted by Dr. Ruey-Hwa Chen, Academia Sinica) were maintained in high-glucose DMEM supplemented with 10% FBS, 100 U mL^{-1} penicillin, 100 µg mL^{-1} streptomycin, and 1 U mL^{-1} GlutaMAX (Gibco, Grand Island, NY, USA). All culture medium was supplemented with Plasmocin (2.5 µg mL^{-1}; InvivoGen, San Diego, CA, USA) to mitigate mycoplasma contamination. Puromycin and Plasmocin were removed for two cell passages prior to subsequent experiments.

Animal studies. Female BALB/c mice were purchased from BioLASCO Taiwan Co., Ltd. (Ilan, Taiwan) for all *in vivo* studies. For euthanasia, 200 µL Zoletil 50 (25 mg mL^{-1}; Sigma-Aldrich, St. Louis, MO, USA) and xylazine (20 mg mL^{-1}; Sigma-Aldrich) were intramuscularly injected into the mouse thighs, followed by cervical relocation. All animals received humane care in compliance with the National Academy of Sciences Guide for the Care and Use of Laboratory Animals. The NTHU Animal Research Committee approved all study procedures and protocols.

Generation of 4T1-PalmGRET, -shCd9, -shCd44, and -shSlc29a1 stable cell lines and EVs. To generate the 4T1-PalmGRET stable cell line, pLenti CMV Puro DEST plasmids encoding PalmGRET (plasmid #158221, Addgene, Watertown, MA, USA) were packaged into

lentiviruses. The 4T1 cells were then transduced with the packaged virus. Non-transduced cells were eliminated with puromycin selection (1 μg mL^{-1}, MDbio, Taipei, Taiwan). Additional selection using fluorescence-activated cell sorting was done to screen for cells that highly expressed PalmGRET.

To generate the 4T1-PalmGRET tpEVSurfMEM KD stable cell lines, pLKO.1 plasmids encoding either shRNA targeting mouse *Cd9* (TRCN0000066396), *Cd44* (TRCN0000262945), or *Slc29a1* (TRCN0000079726) or Scramble (ASN0000000002) from the National RNAi Core Facility (Academia Sinica) were individually packaged into lentiviruses, which were either used directly for experiments or stored in aliquots at −80°C until subsequent experiments. The 4T1-PalmGRET cells were transduced with the packaged lentiviruses to produce stable cell lines with depleted *Cd9*, *Cd44*, or *Slc29a1* expression. The 4T1-PalmGRET-shCd9, -shCd44, -shSlc29a1, and -Scramble cell lines subsequently underwent real-time (RT)-qPCR to examine targeted mRNA expression and were cultured for the KD-EV isolation experiments.

RNA isolation and RT-qPCR. Total RNAs were isolated from stable 4T1-PalmGRET-shCd9, -shCd44, -shSlc29a1, and -Scramble cells using a RNeasy Mini Kit (Qiagen, Hilden, Germany) and underwent RT-qPCR to quantify *Cd9*, *Cd44*, *Slc29a1*, and β-actin mRNA expression. Total RNA was first reverse-transcribed into complementary DNA (cDNA) using a SuperScript™ IV First-Strand Synthesis System (Invitrogen) followed by qPCR with a SYBR Green PCR Master Mix (Invitrogen) using a StepOnePlus Real-Time PCR System (Applied Biosystem: 95°C for 10 min, 40 cycles at 95°C for 15 s, and 62°C for 1 min). The relative gene expressions were calculated using the comparative threshold cycle (ΔΔCT) method. **Table S3** lists the primers used.

Isolation of bEVs and sEVs. The 4T1, 4T1-PalmGRET, MDAMB-231, Hs578T, and BT549 cells were cultured in high-glucose DMEM supplemented with 5% EV-depleted FBS, penicillin (100 U mL^{-1}), and streptomycin (100 μg mL^{-1}). The MCF7 and SKBR3 cells were cultured in high-glucose DMEM supplemented with 5% EV-depleted FBS, penicillin (100 U mL^{-1}), streptomycin (100 μg mL^{-1}), and 1 U mL^{-1} GlutaMAX for 48 h at 37°C with 5% CO_2 in a humidified incubator. CM from cell culture dishes with 80–90% cell confluence was pooled and underwent differential centrifugation, where it was sequentially centrifuged at 300 ×*g* and 2000 ×*g* at 4°C for 10 min to remove cells and cell debris, respectively. Next, the supernatants were centrifuged at 20,000 ×*g* at 4 °C for 30 min, and the bEV pellets were suspended in double 0.22-μm-filtered PBS. The remaining supernatants were subsequently centrifuged at 100,000

×*g* at 4°C for 90 min, and the sEV pellets were suspended in double 0.22-µm-filtered PBS. The harvested bEVs and sEVs were topped up to 5 mL with double 0.22-µm-filtered PBS and centrifuged at 20,000 ×*g* (bEVs) or 100,000 ×*g* (sEVs) at 4°C for 60 min to remove non-EV contaminants. The washed bEV and sEV pellets were suspended in double 0.22-µm-filtered PBS. The protein concentrations of the isolated EVs were determined by a Pierce BCA Kit (Thermo Fisher Scientific, MA, USA). The bEV and sEV samples were either used directly for experiments or stored in aliquots at −80°C.

Lipophilic fluorescent dye labelling. Freshly isolated EVs were labeled with PKH26 (Sigma-Aldrich), DiD, or DiR (Thermo Scientific). PKH26 labeling was performed using the manufacturer's recommended protocol while DiD and DiR labelling was performed using the manufacturer's recommended protocol with minor modifications. Briefly, freshly isolated bEV or sEV samples were incubated with 5 µM DiD or DiR for 20 min at 37°C protected from light. Subsequently, the EV samples were topped up to 5 mL with double 0.22-µm-filtered PBS and centrifuged at 20,000 ×*g* (bEVs) or 100,000 ×*g* (sEVs) at 4°C for 60 min to remove free dye. The washed dyed bEV and sEV pellets were suspended in double 0.22-µm-filtered PBS and were either used directly for experiments or stored in aliquots at −80°C.

NTA. The particle size and concentrations of isolated EVs were determined using a NanoSight NS300 Instrument version 3.2 Dev Build 3.2.16 (Malvern Panalytical, Malvern, UK). Triplicate measurements per sample were made using capture camera level 10 with temperature control at 25 ± 0.01°C.

Sucrose density gradient analysis. For sucrose gradient fractionation, 8%, 30%, 45%, and 60% (w/v) sucrose (Sigma-Aldrich) in PBS (pH 7.4) were layered. The isolated bEVs and sEVs were loaded on top of the discontinuous sucrose gradient, followed by centrifugation at 268,000 ×*g* at 4°C for 38 min with an MLA-50 rotor (Beckman Coulter, Brea, CA, USA). The top layer and subsequent 10 fractions (fractions 1–10) were collected. Of each fraction, 16.5 µL was saved for the BLI assay. Fractions 2–9 were diluted 1:10 in PBS and centrifuged at 20,000 ×*g* (bEVs) or 100,000 ×*g* (sEVs) at 4°C for 1 h with an MLS-55 rotor (Beckman Coulter). The bEV and sEV pellets were suspended in double 0.22-µm-filtered PBS and were either used directly for experiments or stored in aliquots at −80°C until subsequent BLI, NTA, or western blot analyses.

Western blotting. The cells and EVs were lysed in radioimmunoprecipitation assay lysis buffer (1× PBS, pH 7.4, with 1% Igepal CA-630, 0.5% sodium deoxycholate, 0.1% sodium dodecyl sulfate) with cOmplete protease inhibitor cocktail (Roche, Basel, Switzerland). The EV and cell lysate protein concentrations were determined using a Pierce BCA Protein Assay Kit (Thermo Fisher Scientific). The protein lysates were separated using Bolt 4–12% Bis-Tris Plus Gels (Burlington, MA, USA) and transferred onto 0.45-µm polyvinylidene fluoride membranes (Amersham Bioscience, Little Chalfont, UK). The membranes were blocked with 5% bovine serum albumin (BSA, Cyrusbioscience, Taipei, Taiwan) in TBST (1× Tris-buffered saline [TBS, pH 7.4] with 0.1% Tween 20) for 1 h at room temperature and immunoprobed with primary antibodies overnight at 4°C. The membranes were washed three times in TBST at room temperature, incubated with infrared dye-conjugated secondary antibodies for 1 h at room temperature, and imaged by an Odyssey CLx unit (LI-COR Biosciences, Lincoln, NE, USA). **Table S6** lists the information on the primary and secondary antibodies used**.**

Dot blot analysis. The purified EVs were serially diluted to 2000, 1000, 500, and 250 ng in 5 µL 0.22-µm-filtered PBS to characterize the PalmGRET membrane orientation in the bEVs and sEVs. The cell lysates were diluted to 1000 ng in 5 µL 0.22-µm-filtered PBS as positive controls. The diluted bEVs, sEVs, cell lysates, and double 0.22-µm-filtered PBS (all, 5 µL) were dotted onto 0.22-µm nitrocellulose membranes (Amersham Bioscience) and blocked in either TBS (5% BSA w/v) or TBST (5% BSA w/v) overnight at 4°C. The membranes were immunoprobed with anti-GFP antibody (GeneTex, Irvine, CA, USA) diluted in either TBS (5% BSA w/v) or TBST (5% BSA w/v) overnight at 4°C, washed three times in TBS or TBST at 30 min per wash, and incubated with IR dye-conjugated secondary antibodies for 1 h at room temperature and imaged by an Odyssey CLx unit (LI-COR Biosciences). **Table S6** lists the information on the primary and secondary antibodies used.

In Vivo and Ex Vivo Imaging. BALB/c mice were anesthetized after bolus injection of 100 µg of 4T1-PalmGRET-DiR bEV or sEV. Subsequently, 1/40 diluted furimazine (Promega) in 200 µL 0.22-µm-filtered PBS was IV-injected to the mice via tail vein for IVIS imaging. Images were taken at 15 min, 4 h, 48 h post-Fz administration. Following the initial brightfield imaging, PalmGRET signals (via BRET-FL) were obtained using 520 nm emission filter. A 740 nm excitation filter and 800 nm emission filter were used to acquire DiR signals. Following live animal imaging, each mouse was anesthetized again, and euthanized with cervical dislocation. Major organs including the brain, lungs, heart, liver, spleen, kidneys, stomach, intestine, spine,

femur, and fat pad were harvested for ex vivo imaging. The harvested organs were immersed in 1/400 diluted furimazine (Promega) in sterilized PBS and then subjected for IVIS imaging to detect PalmGRET (via BRET-FL; 520 emission filter) and DiR (via exciFL-excited; 740 nm excitation/800 nm emission filters) signals.

MS and proteomics analysis. Polyacrylamide gel slices containing bEV and sEV protein lysates were resolved in 10×10^{-1} M tris (2-carboxyethyl) phosphine (Sigma-Aldrich) with 50×10^{-1} M ammonium bicarbonate (Sigma-Aldrich) for 30 min at 37°C and alkylated in 50×10^{-1} M iodoacetamide (Sigma-Aldrich) with 50×10^{-1} M ammonium bicarbonate for 45 min in the dark at 25°C. Trypsin/Lys-C solution (Promega) was added and incubated at 37°C for 12 h. The resulting peptides were extracted from the gel fragments and analyzed with an Orbitrap Fusion Lumos Mass Spectrometer (Thermo Fisher Scientific) combined with an UltiMate 3000 RSLC nano-flow high-performance liquid chromatography system (Thermo Fisher Scientific) with HCD (higher energy collision dissociation) or EThcD (electron transfer/HCD) MS/MS mode. The MS/MS spectra raw file was processed for peak detection using MaxQuant version 1.6.5.01.[31] Peptides were identified by using the Andromeda search engine and the Swiss-Prot database. EP-HCA1-PalmGRET was searched against the UniProt *Mus musculus* database (Swiss-Prot, 17,009 reviewed protein sequences, UP000000589). The search criteria used were trypsin specificity, fixed modification of carbamidomethyl, and variable modifications of oxidation and acetyl (Protein N-term), and up to two missed cleavages were allowed. A minimum of five amino acids in the peptide length was required. The precursor mass tolerance was 20 ppm and the fragment ion tolerance was 0.5 Da. A false discovery rate of 0.01 and PeptideRank of 1 were set for peptide identification filters. Proteomic data have been submitted to ProteomeXchange.

Bioluminescence assays. A GloMax Discover Microplate Reader (Promega) with auto-injectors was set for Nluc (450/10 nm) and BRET-FL (510/10 nm) readings. The BRET ratio was calculated by dividing the acceptor signal (510/10 nm) by the donor signal (450/10 nm). To assess EV BL, 5 μL EVs (triplicates), 5 μL each fraction (triplicates), or 3 μL pelleted fractions 2–9 (duplicates) were added to a 96-well white plate (Greiner Bio-One, Monroe, NC, USA). The Nluc and BRET signals were measured (integration time: 1 s) after auto-injecting either Fz (Promega) or FFz (Promega) at a 25 M final concentration. For EV biodistribution analysis, the harvested organs were homogenized and lysed by T-PER (0.5 g organ mL^{-1} T-PER, Thermo Fisher Scientific) with 1× Halt protease inhibitor (Thermo Fisher Scientific). The

lysates were centrifuged at 10,000 ×*g* at 4°C for 10 min, followed by supernatant collection to acquire the protein extracts. The supernatants were added to a 96-well white plate (Greiner Bio-One) at 20 μL per well in triplicates. The BL signals were measured after auto-injection of 80 μL FFz (Promega) in PBS per well to achieve a 25 M final concentration with a 1-s integration time.

EV organotropism redirection study by EV membrane modification. BALB/c mice were injected IV with 10 μg 4T1-PalmGRET-shCd9-, -shCd44-, -shSlc29a1-, or -Scramble-bEVs or -sEVs at 0, 24, 48, and 72 h through the tail vein. At 0.5 h and 72.5 h post-injection, the mice were anesthetized, euthanized by cervical dislocation, and dissected to obtain the blood (via cardiac puncture) and organs (brain, lungs, heart, liver, spleen, kidney, stomach, spinal cord, femur, fat pad) for BLI biodistribution analyses. The total RLU per organ was calculated as follows: (RLU/20 μL) × (organ mL^{-1} T-PER lysis buffer). The proportions of the detected EP signal was calculated as follows: (RLU of specific organ)/(RLU of all organs) × 100%.

Murine breast cancer model. Murine 4T1 breast cancer cells were cultured, harvested, and suspended in PBS (pH 7.4). BALB/c mice were anesthetized prior to cancer cell injection. The breast cancer tumor model was established by subcutaneous injection of 100 μL 5×10^4 cells in PBS into the mammary fat pad of 6–8-week-old female BALB/c mice.

Immunohistochemistry. For histological analysis, the tissues were dissected, fixed in 4% paraformaldehyde, and embedded in paraffin. Subsequently, the tissue blocks were cut into 5-μm thick sections. Heat-mediated antigen retrieval with citrate buffer (pH 6.0) was performed on the deparaffinized and rehydrated tissue sections. Next, the sections were washed with TBS-0.025% Triton® X-100, then blocked with TBS containing 1% BSA and 2% normal goat serum for 1 h at room temperature. The sections were incubated with primary antibodies in a humidified chamber at 4°C overnight, washed with TBS-0.025% Triton® X-100, and incubated with Alexa Fluor 568-conjugated secondary antibody for 1 h at room temperature. Subsequently, autofluorescence was quenched using a Vector® TrueVIEW® Autofluorescence Quenching Kit (Vector Laboratories, Newark, CA, USA). The sections were washed with PBS and mounted using VECTASHIELD® Vibrance™ mounting media with 4′,6-diamidino-2-phenylindole (DAPI, Vector Laboratories). **Table S6** lists the primary and secondary antibody dilutions for the organ tissues. All tissue sections were imaged using an LSM 980 Airyscan 2 confocal laser scanning microscope (Zeiss, Stuttgart, Germany) under similar imaging

parameters. The images were acquired and processed using ZEN blue 3.3 (Zeiss). EV quantitative analyses were performed using Fiji (ImageJ, NIH) under similar threshold settings.

Statistical analyses. Statistical analyses were performed using GraphPad Prism 7.05. A 2-tailed Student's t-test was used for comparison between two groups. One-way analysis of variance (ANOVA) followed by Tukey's or Dunnett's post hoc test was used for comparison of ≥3 groups. The values were normally distributed and the variance was similar between compared groups. Error bars for all graphs represent the mean ± SEM. $P < 0.05$ was considered statistically significant.

Supporting Information

Supporting Information is available from the Wiley Online Library or from the author.

Acknowledgements

The authors thank Dr. Wei Chun Huang (Biophysics Core Facility, Institute of Atomic and Molecular Sciences, Academia Sinica) for assistance and technical support, Chia Chen Tai and Tzu Wen Tai [Flow Cytometry Core Facility, Academia Sinica Core Facility and Innovative Instrument Project (AS-CFII 108-113)] for assistance on the cell sorting service, the National RNAi Core Facility (Academia Sinica) for providing the shRNA plasmids, Dr. Hsin-Yi Wu (NTU Consortia of Key Technologies and NTU Instrumentation Center) for providing mass spectrometry technical research services, and the NTHU Biomedical Science & Engineering Center Animal Care Facility. The Lai Lab was supported by the National Science and Technology Council (NSTC) under Grant Nos. 111-2628-B-001-004 (C.P.L.) and 111-2628-B-001-022 (C.P.L.), Academia Sinica Innovative Materials and Analysis Technology Exploration (iMATE) Program AS-iMATE-111-34 (C.P.L.), Academia Sinica Career Development Award AS-CDA-109-M04 (C.P.L.). Yen-Ju Chen and Anthony Yan-Tang Wu contributed equally to this work.

References

[1] a)B. T. Pan, K. Teng, C. Wu, M. Adam, R. M. Johnstone, *The Journal of Cell Biology* **1985**, 101, 942; b)M. Tkach, C. Théry, *Cell* **2016**, 164, 1226.

[2] C. Théry, K. W. Witwer, E. Aikawa, M. J. Alcaraz, J. D. Anderson, R. Andriantsitohaina, A. Antoniou, T. Arab, F. Archer, G. K. Atkin-Smith, D. C. Ayre, J.-M. Bach, D. Bachurski, H. Baharvand, L. Balaj, S. Baldacchino, N. N. Bauer, A. A. Baxter, M. Bebawy, C. Beckham, A. Bedina Zavec, A. Benmoussa, A. C. Berardi, P. Bergese, E. Bielska, C. Blenkiron, S. Bobis-Wozowicz, E. Boilard, W. Boireau, A. Bongiovanni, F. E. Borràs, S. Bosch, C. M. Boulanger, X. Breakefield, A. M. Breglio, M. Á. Brennan, D. R. Brigstock, A. Brisson, M. L. Broekman, J. F. Bromberg, P. Bryl-Górecka, S. Buch, A. H. Buck, D. Burger, S. Busatto, D. Buschmann, B. Bussolati, E. I. Buzás, J. B. Byrd, G. Camussi, D. R. Carter, S. Caruso, L. W. Chamley, Y.-T. Chang, C. Chen, S. Chen, L. Cheng, A. R. Chin, A. Clayton, S. P. Clerici, A. Cocks, E. Cocucci, R. J. Coffey, A. Cordeiro-da-Silva, Y. Couch, F. A. Coumans, B. Coyle, R. Crescitelli, M. F. Criado, C. D'Souza-Schorey, S. Das, A. Datta Chaudhuri, P. de Candia, E. F. De Santana, O. De Wever, H. A. del Portillo, T. Demaret, S. Deville, A. Devitt, B. Dhondt, D. Di Vizio, L. C. Dieterich, V. Dolo, A. P. Dominguez Rubio, M. Dominici, M. R. Dourado, T. A. Driedonks, F. V. Duarte, H. M. Duncan, R. M. Eichenberger, K. Ekström, S. EL Andaloussi, C. Elie-Caille, U. Erdbrügger, J. M. Falcon-Perez, F. Fatima, J. E. Fish, M. Flores-Bellver, A. Försönits, A. Frelet-Barrand, F. Fricke, G. Fuhrmann, S. Gabrielsson, A. Gámez-Valero, C. Gardiner, K. Gärtner, R. Gaudin, Y. S. Gho, B. Giebel, C. Gilbert, M. Gimona, I. Giusti, D. C. Goberdhan, A. Görgens, S. M. Gorski, D. W. Greening, J. C. Gross, A. Gualerzi, G. N. Gupta, D. Gustafson, A. Handberg, R. A. Haraszti, P. Harrison, H. Hegyesi, A. Hendrix, A. F. Hill, F. H. Hochberg, K. F. Hoffmann, B. Holder, H. Holthofer, B. Hosseinkhani, G. Hu, Y. Huang, V. Huber, S. Hunt, A. G.-E. Ibrahim, T. Ikezu, J. M. Inal, M. Isin, A. Ivanova, H. K. Jackson, S. Jacobsen, S. M. Jay, M. Jayachandran, G. Jenster, L. Jiang, S. M. Johnson, J. C. Jones, A. Jong, T. Jovanovic-Talisman, S. Jung, R. Kalluri, S.-I. Kano, S. Kaur, Y. Kawamura, E. T. Keller, D. Khamari, E. Khomyakova, A. Khvorova, P. Kierulf, K. P. Kim, T. Kislinger, M. Klingeborn, D. J. Klinke, M. Kornek, M. M. Kosanović, Á. F. Kovács, E.-M. Krämer-Albers, S. Krasemann, M. Krause, I. V. Kurochkin, G. D. Kusuma, S. Kuypers, S. Laitinen, S. M. Langevin, L. R. Languino, J. Lannigan, C. Lässer, L. C. Laurent, G. Lavieu, E. Lázaro-Ibáñez, S. Le Lay, M.-S. Lee, Y. X. F. Lee, D. S. Lemos, M. Lenassi, A. Leszczynska, I. T. Li, K. Liao, S. F. Libregts, E. Ligeti, R. Lim, S. K. Lim, A. Linē, K. Linnemannstöns, A. Llorente, C. A. Lombard, M. J. Lorenowicz, Á. M. Lörincz, J. Lötvall, J. Lovett, M. C. Lowry, X. Loyer, Q. Lu, B. Lukomska, T. R. Lunavat, S. L. Maas, H. Malhi, A. Marcilla, J. Mariani, J. Mariscal, E. S. Martens-Uzunova, L. Martin-Jaular, M. C. Martinez, V. R. Martins, M. Mathieu, S. Mathivanan, M. Maugeri, L. K. McGinnis, M. J. McVey, D. G. Meckes, K. L. Meehan, I. Mertens, V. R. Minciacchi, A. Möller, M. Møller Jørgensen, A. Morales-Kastresana, J. Morhayim, F. Mullier, M. Muraca, L. Musante, V. Mussack, D. C. Muth, K. H. Myburgh, T. Najrana, M. Nawaz, I. Nazarenko, P. Nejsum, C. Neri, T. Neri, R. Nieuwland, L. Nimrichter, J. P. Nolan, E. N. Nolte-'t Hoen, N. Noren Hooten, L. O'Driscoll, T. O'Grady, A. O'Loghlen, T. Ochiya, M. Olivier, A. Ortiz, L. A. Ortiz, X. Osteikoetxea, O. Østergaard, M. Ostrowski, J. Park, D. M. Pegtel, H. Peinado, F. Perut, M. W. Pfaffl, D. G. Phinney, B. C. Pieters, R. C. Pink, D. S. Pisetsky, E. Pogge von Strandmann, I. Polakovicova, I. K. Poon, B. H. Powell, I. Prada, L. Pulliam, P. Quesenberry, A. Radeghieri, R. L. Raffai, S. Raimondo, J. Rak, M. I. Ramirez, G. Raposo, M. S. Rayyan, N. Regev-Rudzki, F. L. Ricklefs, P. D. Robbins, D. D. Roberts, S. C. Rodrigues, E. Rohde, S. Rome, K. M. Rouschop, A. Rughetti, A. E. Russell, P. Saá, S. Sahoo, E. Salas-Huenuleo, C. Sánchez, J. A. Saugstad, M. J. Saul, R. M. Schiffelers, R. Schneider, T. H. Schøyen, A. Scott, E. Shahaj, S. Sharma, O. Shatnyeva, F. Shekari, G. V. Shelke, A. K. Shetty, K. Shiba, P. R.-M. Siljander, A. M. Silva, A. Skowronek, O. L. Snyder, R. P. Soares, B. W. Sódar, C. Soekmadji, J. Sotillo, P. D. Stahl, W. Stoorvogel, S. L. Stott, E.

F. Strasser, S. Swift, H. Tahara, M. Tewari, K. Timms, S. Tiwari, R. Tixeira, M. Tkach, W. S. Toh, R. Tomasini, A. C. Torrecilhas, J. P. Tosar, V. Toxavidis, L. Urbanelli, P. Vader, B. W. van Balkom, S. G. van der Grein, J. Van Deun, M. J. van Herwijnen, K. Van Keuren-Jensen, G. van Niel, M. E. van Royen, A. J. van Wijnen, M. H. Vasconcelos, I. J. Vechetti, T. D. Veit, L. J. Vella, É. Velot, F. J. Verweij, B. Vestad, J. L. Viñas, T. Visnovitz, K. V. Vukman, J. Wahlgren, D. C. Watson, M. H. Wauben, A. Weaver, J. P. Webber, V. Weber, A. M. Wehman, D. J. Weiss, J. A. Welsh, S. Wendt, A. M. Wheelock, Z. Wiener, L. Witte, J. Wolfram, A. Xagorari, P. Xander, J. Xu, X. Yan, M. Yáñez-Mó, H. Yin, Y. Yuana, V. Zappulli, J. Zarubova, V. Žėkas, J.-Y. Zhang, Z. Zhao, L. Zheng, A. R. Zheutlin, A. M. Zickler, P. Zimmermann, A. M. Zivkovic, D. Zocco, E. K. Zuba-Surma, *Journal of Extracellular Vesicles* **2018**, 7, 1535750.

[3] K. Brennan, K. Martin, S. P. FitzGerald, J. O'Sullivan, Y. Wu, A. Blanco, C. Richardson, M. M. Mc Gee, *Scientific Reports* **2020**, 10, 1039.

[4] H. Zhang, D. Lyden, *Nature Protocols* **2019**, 14, 1027.

[5] J. W. Clancy, A. C. Boomgarden, C. D'Souza-Schorey, *Nature Cell Biology* **2021**, 23, 1217.

[6] C. Ciardiello, A. Leone, P. Lanuti, M. S. Roca, T. Moccia, V. R. Minciacchi, M. Minopoli, V. Gigantino, R. De Cecio, M. Rippa, L. Petti, F. Capone, C. Vitagliano, M. R. Milone, B. Pucci, R. Lombardi, F. Iannelli, E. Di Gennaro, F. Bruzzese, M. Marchisio, M. V. Carriero, D. Di Vizio, A. Budillon, *Journal of Experimental & Clinical Cancer Research* **2019**, 38, 317.

[7] R. Kalluri, V. S. LeBleu, *Science* **2020**, 367, eaau6977.

[8] K. Menck, S. Sivaloganathan, A. Bleckmann, C. Binder, *Int J Mol Sci* **2020**, 21.

[9] N. Kastelowitz, H. Yin, *ChemBioChem* **2014**, 15, 923.

[10] a)F. Heitz, P. Harter, H. J. Lueck, A. Fissler-Eckhoff, F. Lorenz-Salehi, S. Scheil-Bertram, A. Traut, A. du Bois, *Eur J Cancer* **2009**, 45, 2792; b)M. Riaz, M. T. M. van Jaarsveld, A. Hollestelle, W. J. C. Prager-van der Smissen, A. A. J. Heine, A. W. M. Boersma, J. Liu, J. Helmijr, B. Ozturk, M. Smid, E. A. Wiemer, J. A. Foekens, J. W. M. Martens, *Breast Cancer Research* **2013**, 15, R33; c)A. Naderi, A. E. Teschendorff, N. L. Barbosa-Morais, S. E. Pinder, A. R. Green, D. G. Powe, J. F. Robertson, S. Aparicio, I. O. Ellis, J. D. Brenton, C. Caldas, *Oncogene* **2007**, 26, 1507; d)X. Dai, H. Cheng, Z. Bai, J. Li, ... *Journal of Cancer* **2017**, 8, 3131.

[11] O. Yersal, S. Barutca, *World Journal of Clinical Oncology* **2014**, 5, 412.

[12] a)L. Wang, B. Wang, H. Wen, J. Mao, Y. Ren, H. Yang, *Oncol Rep* **2020**, 44, 407; b)S. Dutta, C. Warshall, C. Bandyopadhyay, D. Dutta, B. Chandran, *PLoS One* **2014**, 9, e97580; c)S. Lucotti, C. M. Kenific, H. Zhang, D. Lyden, *EMBO J* **2022**, 41, e109288; d)J. Peng, W. Wang, S. Hua, L. Liu, *Breast Cancer (Auckl)* **2018**, 12, 1178223418767666.

[13] a)S. T. Chuo, J. C. Chien, C. P. Lai, *J Biomed Sci* **2018**, 25, 91; b)F. J. Verweij, L. Balaj, C. M. Boulanger, D. R. F. Carter, E. B. Compeer, G. D'Angelo, S. E. L. Andaloussi, J. G. Goetz, J. C. Gross, V. Hyenne, E.-M. Krämer-Albers, C. P. Lai, X. Loyer, A. Marki, S. Momma, E. N. M. N.-t. Hoen, D. M. Pegtel, H. Peinado, G. Raposo, K. Rilla, H. Tahara, C. Théry, M. E. v. Royen, R. E. Vandenbroucke, A. M. Wehman, K. Witwer, Z. Wu, R. Wubbolts, G. v. Niel, *Nature Methods* **2021**, 18, 1013

[14] a)M. Dehghani, S. M. Gulvin, J. Flax, T. R. Gaborski, *Scientific Reports* **2020**, 1; b)A. Y.-T. Wu, Y.-C. Sung, Y. J. Chen, S. T. Y. Chou, V. Guo, J. C.-Y. Chien, J. J.-S. Ko, A. L. Yang, H. C. Huang, J. C. Chuang, S. Wu, M. R. Ho, M. Ericsson, W.-W. Lin, C. H. Y. Cheung, H. F. Juan, K. Ueda, Y. Chen, C. P.-K. Lai, *Advanced Science* **2020**, 7, 2001467.

[15] E. Lázaro-Ibáñez, F. N. Faruqu, A. F. Saleh, A. M. Silva, J. Tzu-Wen Wang, J. Rak, K. T. Al-Jamal, N. Dekker, *ACS nano* **2021**, 15, 3212.

[16] N. G. Zhegalova, S. He, H. Zhou, D. M. Kim, M. Y. Berezin, *Contrast Media Mol Imaging* **2014**, 9, 355.

[17] a)G. F. Teare, P. K. Horan, S. E. Slezak, C. Smith, J. B. Hay, *Cell Immunol* **1991**, 134, 157; b)M. Nowacki, L. Nazarewski, M. Pokrywczynska, T. Kloskowski, D. Tyloch, K. Pietkun, A. Jundzill, M. Rasmus, K. Warda, M. Gagat, A. Grzanka, M. Bodnar, A. Marszalek, M. Krawczyk, S. L. Habib, T. Drewa, *Ann Transplant* **2015**, 20, 132; c)D. P. Kuffler, *J Comp Neurol* **1990**, 302, 729.
[18] a)T. Smyth, M. Kullberg, N. Malik, P. Smith-Jones, M. W. Graner, T. J. Anchordoquy, *Journal of controlled release : official journal of the Controlled Release Society* **2015**, 199, 145; b)O. P. Wiklander, J. Z. Nordin, A. O'Loughlin, Y. Gustafsson, G. Corso, I. Mager, P. Vader, Y. Lee, H. Sork, Y. Seow, N. Heldring, L. Alvarez-Erviti, C. I. Smith, K. Le Blanc, P. Macchiarini, P. Jungebluth, M. J. Wood, S. E. Andaloussi, *J Extracell Vesicles* **2015**, 4, 26316.
[19] D. Gupta, A. Maria Zickler, S. EL Andaloussi, *Advanced Drug Delivery Reviews* **2021**, 113961.
[20] a)A. Hoshino, B. Costa-Silva, T.-L. Shen, G. Rodrigues, A. Hashimoto, M. T. Mark, H. Molina, S. Kohsaka, A. D. Giannatale, S. Ceder, S. Singh, C. Williams, N. Soplop, K. Uryu, L. Pharmer, T. King, L. Bojmar, A. E. Davies, Y. Ararso, T. Zhang, H. Zhang, J. Hernandez, J. M. Weiss, V. D. Dumont-Cole, K. Kramer, L. H. Wexler, A. Narendran, G. K. Schwartz, J. H. Healey, P. Sandstrom, K. J. Labori, E. H. Kure, P. M. Grandgenett, M. A. Hollingsworth, M. d. Sousa, S. Kaur, M. Jain, K. Mallya, S. K. Batra, W. R. Jarnagin, M. S. Brady, O. Fodstad, V. Muller, K. Pantel, A. J. Minn, M. J. Bissell, B. A. Garcia, Y. Kang, V. K. Rajasekhar, C. M. Ghajar, I. Matei, H. Peinado, J. Bromberg, D. Lyden, *Nature* **2015**, 527, 329 ; b)H. Choi, Y. Choi, H. Y. Yim, A. Mirzaaghasi, J.-K. Yoo, C. Choi, *Tissue Engineering and Regenerative Medicine* **2021**, 1.
[21] a)J. Mallegol, G. Van Niel, C. Lebreton, Y. Lepelletier, C. Candalh, C. Dugave, J. K. Heath, G. Raposo, N. Cerf-Bensussan, M. Heyman, *Gastroenterology* **2007**, 132, 1866; b)S. Rana, S. Yue, D. Stadel, M. Zöller, *The International Journal of Biochemistry & Cell Biology* **2012**; c)E. Segura, C. Guérin, N. Hogg, S. Amigorena, C. Théry, *J Immunol* **2007**, 179, 1489.
[22] a)M. Logozzi, A. De Milito, L. Lugini, M. Borghi, L. Calabrò, M. Spada, M. Perdicchio, M. L. Marino, C. Federici, E. Iessi, D. Brambilla, G. Venturi, F. Lozupone, M. Santinami, V. Huber, M. Maio, L. Rivoltini, S. Fais, *PLoS ONE* **2009**, 4, e5219; b)M. P. Bebelman, M. J. Smit, D. M. Pegtel, S. R. Baglio, *Pharmacol Ther* **2018**, 188, 1.
[23] B. Bondhopadhyay, S. Sisodiya, F. A. Alzahrani, M. A. Bakhrebah, A. Chikara, V. Kasherwal, A. Khan, J. Rani, S. A. Dar, N. Akhter, P. Tanwar, U. Agrawal, S. Hussain, *Cancers (Basel)* **2021**, 13.
[24] a)F. X. Schaub, M. S. Reza, C. A. Flaveny, W. Li, A. M. Musicant, S. Hoxha, M. Guo, J. L. Cleveland, A. L. Amelio, *Cancer Research* **2015**, 75, 5023; b)N. Gaspar, J. R. Walker, G. Zambito, K. Marella-Panth, C. Lowik, T. A. Kirkland, L. Mezzanotte, *Journal of Photochemistry & Photobiology, B: Biology* **2021**, 216, 112128.
[25] L. Santucci, M. Bruschi, G. Del Zotto, F. Antonini, G. M. Ghiggeri, I. Panfoli, G. Candiano, *Sci Rep* **2019**, 9, 13048.
[26] P. K. Wallace, J. D. T. Jr, J. L. Fisher, S. S. Wallace, M. S. Ernstoff, K. A. Muirhead, *Cytometry Part A* **2008**, 73A, 1019
[27] R. M. Abra, C. A. Hunt, *Biochimica et Biophysica Acta (BBA) - Lipids and Lipid Metabolism* **1981**, 666, 493.
[28] a)J. Wu, P. Liu, J. L. Zhu, S. Maddukuri, M. A. Zern, *Hepatology* **1998**, 27, 772; b)K. McEuen, J. Borlak, W. Tong, M. Chen, *Int J Mol Sci* **2017**, 18.
[29] S. W. Wen, J. Sceneay, L. G. Lima, C. S. F. Wong, M. Becker, S. Krumeich, R. J. Lobb, V. Castillo, K. N. Wong, S. Ellis, B. S. Parker, A. Möller, *Cancer Research* **2016**, 76, 6816.
[30] S. McFarlane, J. A. Coulter, P. Tibbits, A. O'Grady, C. McFarlane, N. Montgomery, A. Hill, H. O. McCarthy, L. S. Young, E. W. Kay, C. M. Isacke, D. J. Waugh, *Oncotarget* **2015**, 6, 11465.

[31] J. Cox, M. Mann, *Nature Biotechnology* **2008**, 26, 1367.
[32] H. Kalra, G. P. C. Drummen, S. Mathivanan, *International Journal of Molecular Sciences* **2016**, 17.

Table of Contents

*Bryan John Abel Magoling, Yen-Ju Chen, Anthony Yan-Tang Wu, Wendy Wan-Ting Wong, Steven Ting-Yu Chuo, Hsi-Chien Huang, Yun-Chieh Sung, Hsin Tzu Hsieh, Poya Huang, Kang-Zhang Lee, Kuan-Wei Huang, Ruey-Hwa Chen, Yunching Chen, Charles Pin-Kuang Lai**

Membrane Protein Modification Modulates Big and Small Extracellular Vesicle Biodistribution and Tumorigenic Potential in Breast Cancers *in vivo*

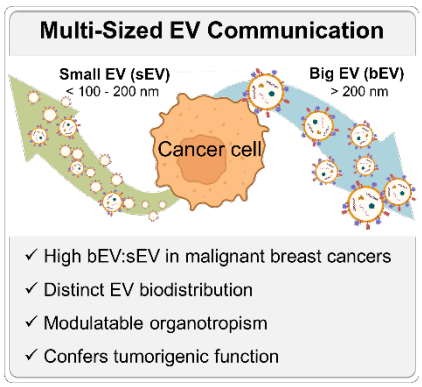

Big and small extracellular vesicles circulate differentially and confer tumorigenic function modulatable by EV membrane proteins. Malignant breast cancers release more bEV, in addition to sEVs, than normal cells to target organs and individually promote tumor growth *via* tumor progression-associated EV surface membrane proteins (tpEVSurfMEMs).

Supporting Information

Membrane Protein Modification Modulates Big and Small Extracellular Vesicle Biodistribution and Tumorigenic Potential in Breast Cancers *in vivo*

*Bryan John Abel Magoling, Yen-Ju Chen, Anthony Yan-Tang Wu, Wendy Wan-Ting Wong, Steven Ting-Yu Chuo, Hsi-Chien Huang, Yun-Chieh Sung, Hsin Tzu Hsieh, Poya Huang, Kang-Zhang Lee, Kuan-Wei Huang, Ruey-Hwa Chen, Yunching Chen, Charles Pin-Kuang Lai**

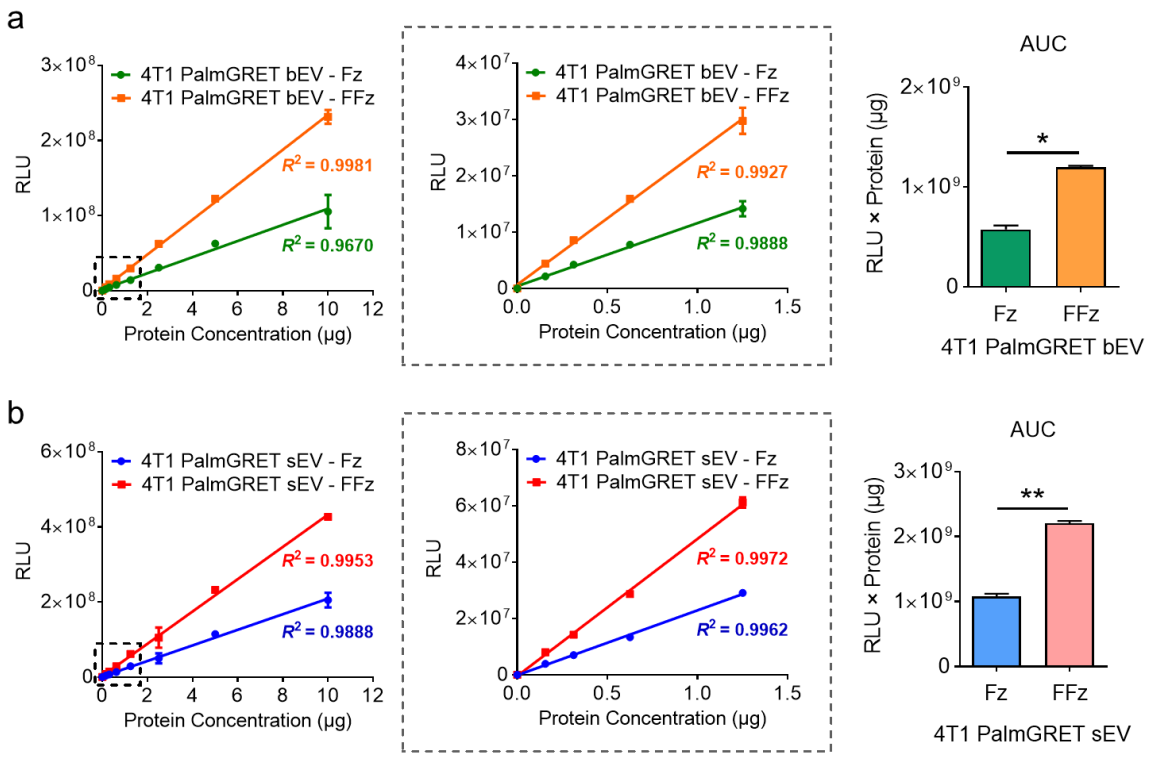

Supporting Figure 1. FFz yields a higher BLI signal in PalmGRET EVs. The plot of Nluc activity vs. protein concentration of **(a)** bEVs and **(b)** sEVs showing significantly increased BLI signals when FFz was applied as compared to Fz. FFz yielded Nluc signals that were ~2-fold higher than that induced by Fz. Both Fz- and FFz-induced Nluc signals were detected in an EV protein concentration-dependent manner and with high correlation in both bEV and sEV samples ($R^2 \geq$~0.99). *$p < 0.05$; **$p < 0.01$ with 2-tailed Student's *t*-test.

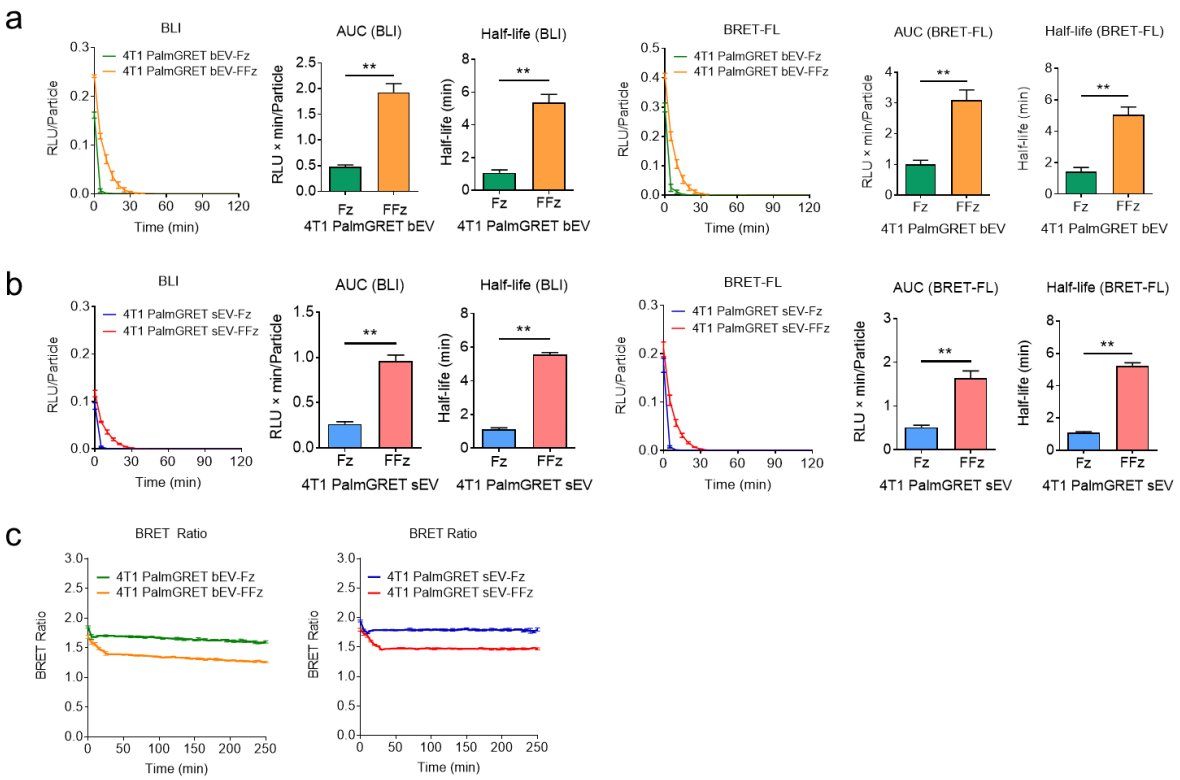

Supporting Figure 2. FFz yields a longer half-life of BLI and BRET-FL signals in PalmGRET EVs. The BLI and BRET-FL of **(a)** bEVs and **(b)** sEVs demonstrated significantly increased BLI half-life when FFz was used as compared to Fz. **c)** The BRET ratio of bEVs and sEVs when reacted with FFz and Fz. Compared to Fz-induced activity, the BRET ratio of FFz-induced signals decreased steadily for the first 30 min before plateauing, which suggested increased enzyme–substrate interaction between Nluc and FFz and hence greater substrate consumption over time than Fz. *$p < 0.05$; **$p < 0.01$; ***$p < 0.001$ with 2-tailed Student's *t*-test.

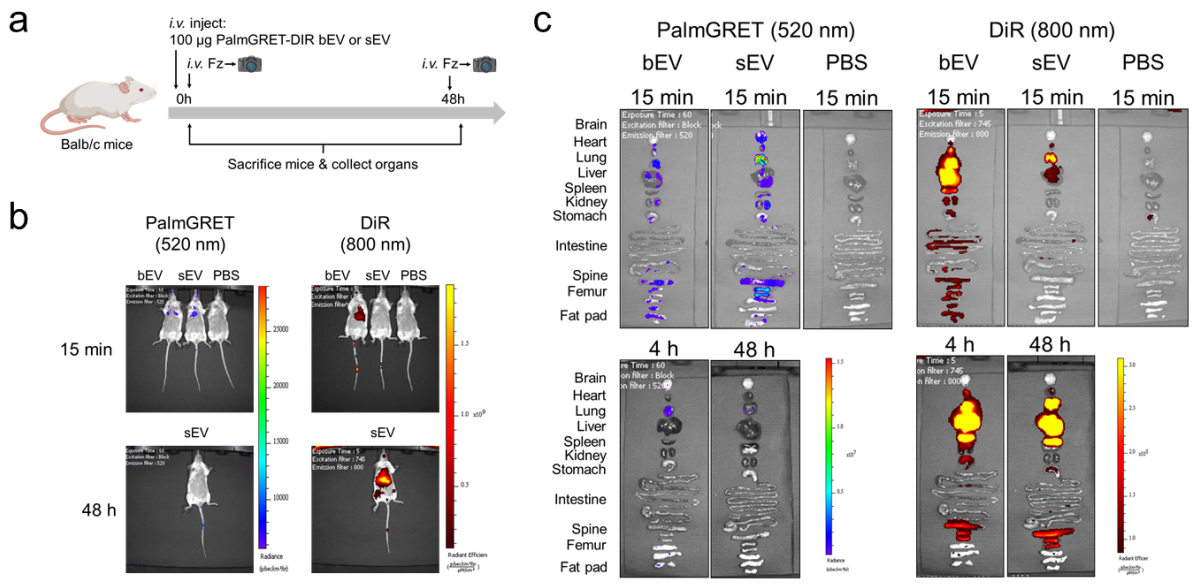

Supporting Figure 3. *In vivo* imaging of 4T1-PalmGRET-DiR-bEVs and -sEVs. a, Schematic of live animal and *ex vivo* imaging of BALB/c mice injected IV with 4T1-PalmGRET-DiR-bEVs and -sEVs. **b,** *In vivo* and **(c)** *ex vivo* images of BALB/c mice administered with 4T1-PalmGRET-DiR-bEVs and -sEVs at 15 min, 4 h, and 48 h post-injection.

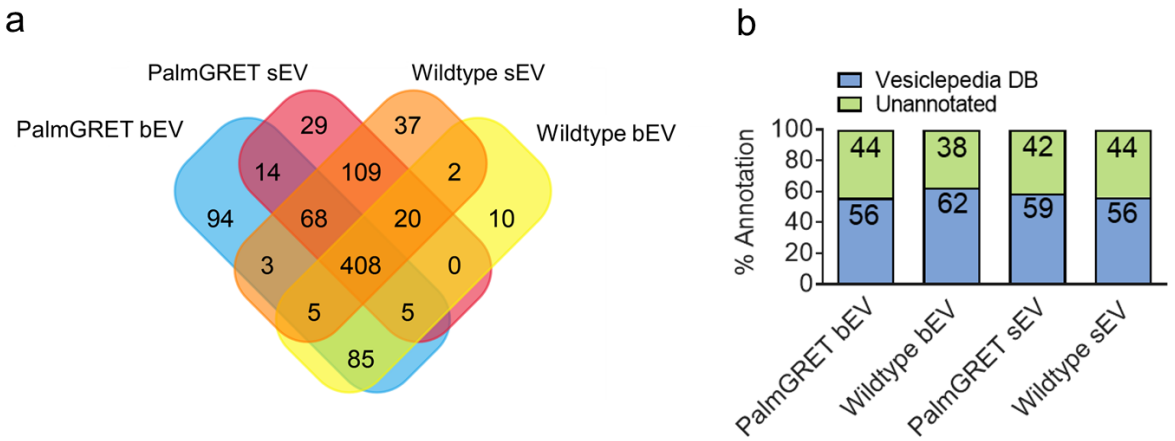

Supporting Figure 4. Proteomic analysis of bEVs and sEVs derived from TNBC 4T1 cells. a, Venn diagram showing unique and common proteins between 4T1-PalmGRET-bEVs and -sEVs and 4T1-WT-bEV and -sEV proteomes. **b,** Bar graph showing the percentage of proteins in each proteome group previously reported in the Vesiclepedia EV database.[32]

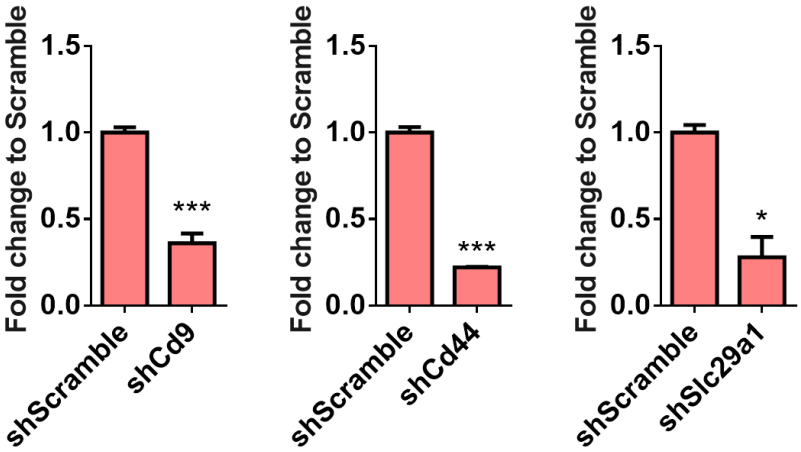

Supporting Figure 5. tpEVSurfMEM transcript KD in 4T1-PalmGRET cells. RT-qPCR indicating reduced relative cDNA expression of *CD9*, *CD44*, and *SLC29A1* in the shCd9, shCd44, and shSlc29a1 groups, respectively, as compared to the Scramble controls. *$p < 0.05$; ***$p < 0.001$ with the 2-tailed Student's *t*-test.

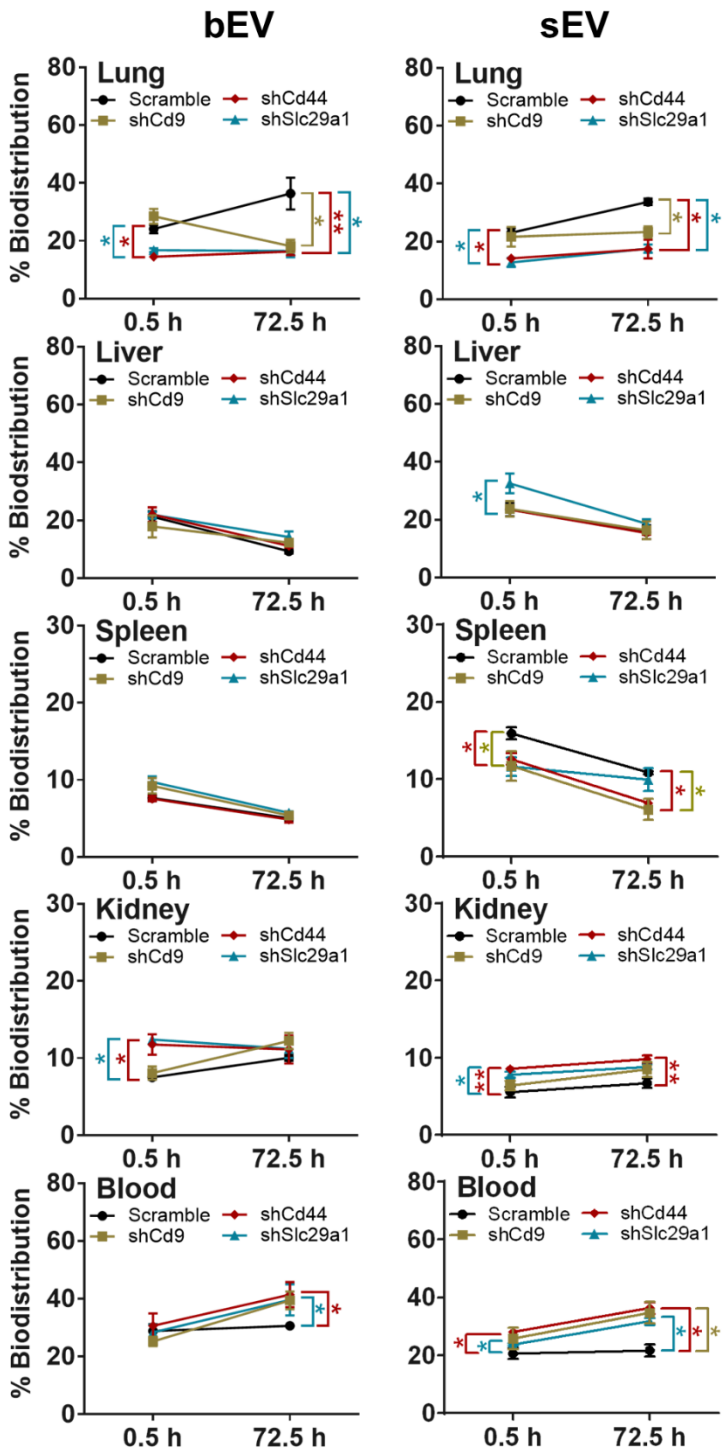

Supporting Figure 6. Biodistribution percentage of 4T1-PalmGRET with tpEVSurfMEM KDs in non-tumor bearing mice. Biodistribution percentage of IV-injected shCd9-, shCd44-, and Slc29a1-4T1-PalmGRET-bEV (left) and -sEV (right) distribution in the lung, liver, kidney, spleen, and blood as compared to the Scramble controls. *$p < 0.05$; **$p < 0.01$ with 2-way ANOVA followed by Dunnett's post hoc test vs. Scramble controls.

a

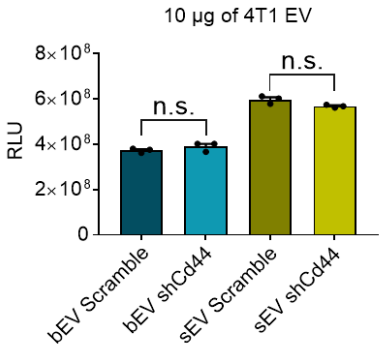
10 μg of 4T1 EV
RLU
8×10^8
6×10^8
4×10^8
2×10^8
0
n.s.
n.s.
bEV Scramble
bEV shCd44
sEV Scramble
sEV shCd44

b

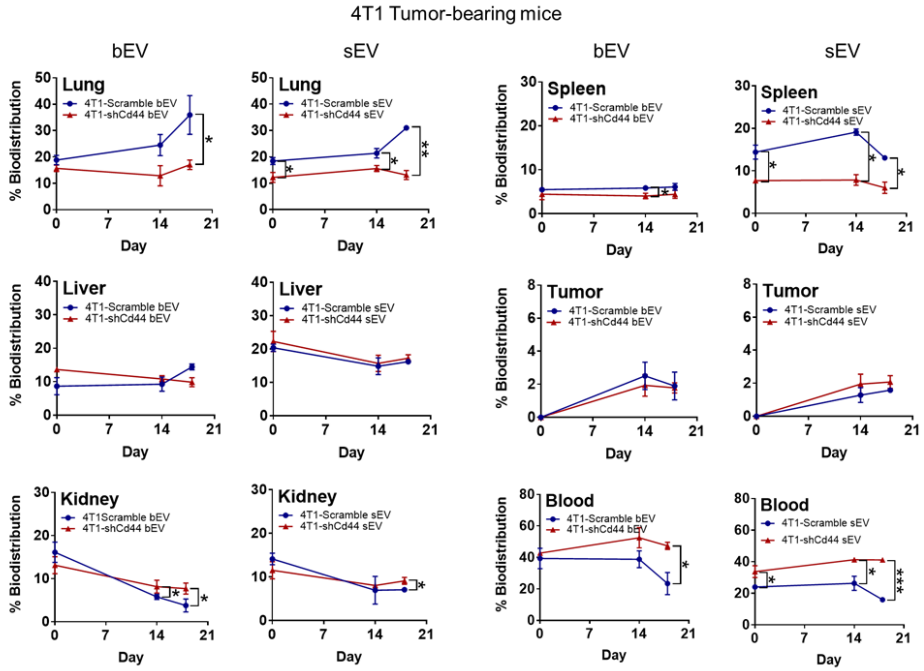
4T1 Tumor-bearing mice
bEV
sEV
bEV
sEV
Lung
Spleen
Liver
Tumor
Kidney
Blood
% Biodistribution
Day
4T1-Scramble bEV
4T1-shCd44 bEV
4T1-Scramble sEV
4T1-shCd44 sEV

c

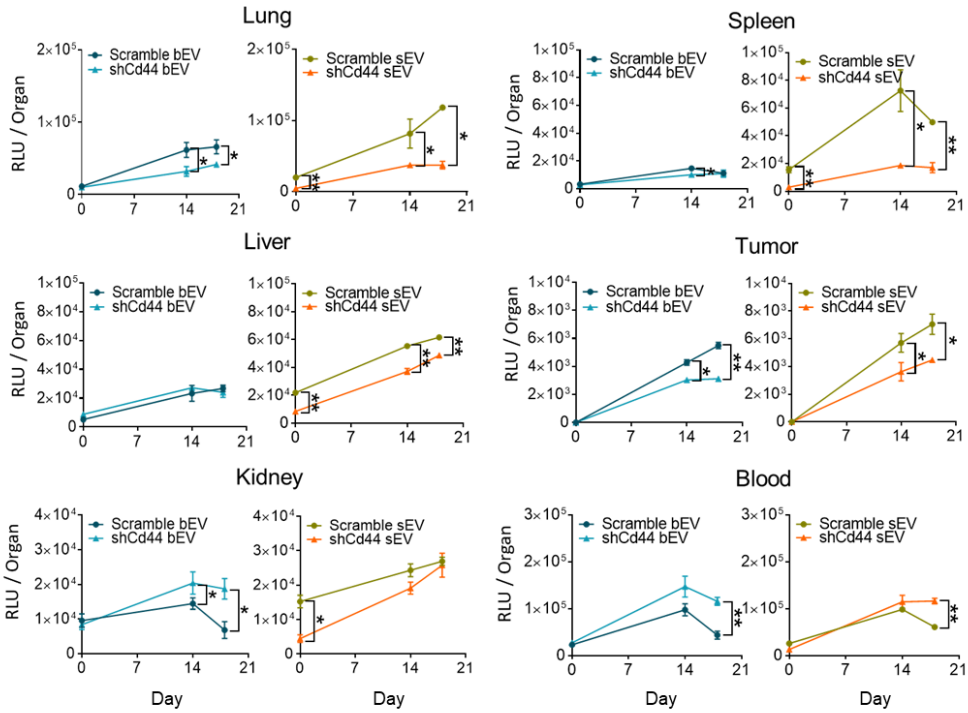
Lung
Spleen
Liver
Tumor
Kidney
Blood
RLU / Organ
Day
Scramble bEV
shCd44 bEV
Scramble sEV
shCd44 sEV

Supporting Figure 7. BLI intensity and biodistribution percentage of 4T1-PalmGRET-EVs with Scramble or shCd44 in 4T1-tumor bearing mice. a) Initial BLI intensity was similar between IV-administered shCd44 and Scramble 4T1-PalmGRET-bEVs and sEVs. **b)** Biodistribution percentage of IV-injected 4T1-PalmGRET-shCd44-bEVs (left) and -sEVs (right) as compared with Scramble controls. *$p < 0.05$; **$p < 0.01$ with 2-tailed Student's *t*-test. n.s., $p > 0.5$; *$p < 0.05$; **$p < 0.01$; ***$p < 0.001$ with 1-way ANOVA followed by multiple group comparisons. **c)** Total EV signal per organ of IV-injected 4T1-PalmGRET-shCd44-bEVs and -sEVs as compared with the Scramble controls.

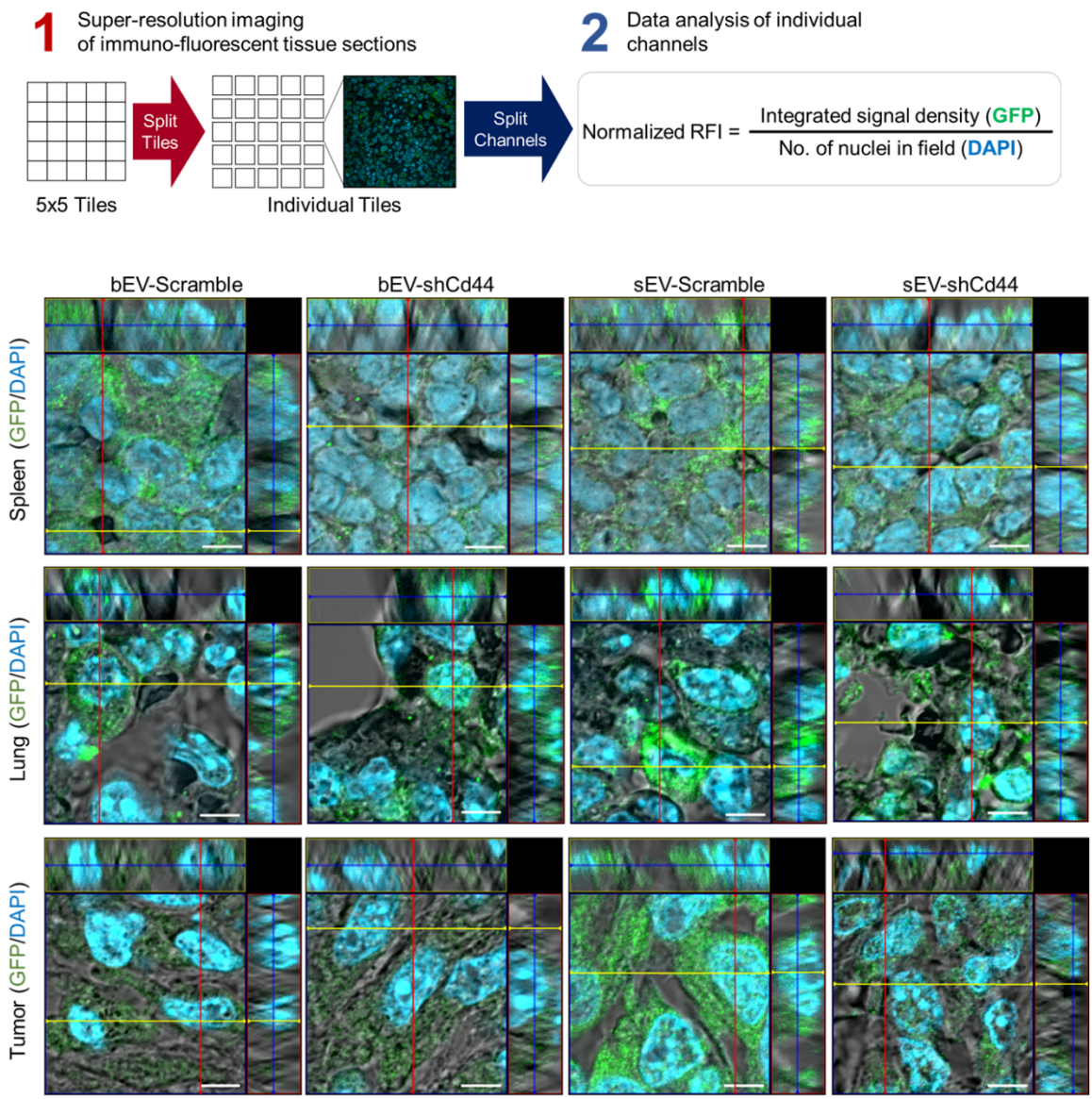

Supporting Figure 8. Cellular uptake of 4T1-PalmGRET-EVs shCd44 with Scramble or shCd44 in 4T1-tumor bearing mice. Orthogonal view of Z-stack images showing intracellular uptake of bEVs and sEVs in the spleen, lung, and tumor of mice treated with

4T1-PalmGRET-Scramble or -shCd44-bEVs or -sEVs at day 18 post-EV treatment. The nuclei were stained by DAPI and 4T1-PalmGRET was immunoprobed by anti-GFP antibody followed by Alexa Fluor 568-conjugated secondary antibody. Bar, 5 μm

Supporting Table 1. Fluorescence Intensity (DiR Channel: 800 nm) of 4T1-PamGRET-DiR bEV and sEV at 0.5 H and 24 H post-injection.

	4TI-PalmGRET bEV (DiR Channel: 800 nm)				**4TI-PalmGRET sEV (DiR Channel: 800 nm)**			
	10 µg		**25 µg**		**10 µg**		**25 µg**	
	0.5H	**24H**	**0.5H**	**24H**	**0.5H**	**24H**	**0.5H**	**24H**
Organ	Ave FI±SEM	Ave FI±SEM	Ave FI±SEM	Ave FI±SEM	Ave FI±SEM	Ave FI±SEM	Ave FI±SEM	Ave FI±SEM
Brain	664±3.04	120±1.25	384±2.72	866±2.63	675±1.60	107±1.59	376±4.50	850±0.71
Lung	800±6.11	951±10.61	3405±9.15	2997±13.02	560±2.80	305±2.50	1942±8.65	3474±14.69
Heart	227±0.21	33±0.24	181±4.63	265±2.18	237±1.40	27±2.54	378±4.63	375±5.86
Liver	28987±11.74	33635±31.77	49185±26.18	83817±25.13	18616±40.50	20006±30.69	17072±31.47	45839±27.33
Spleen	1711±8.07	841±1.66	1636±6.58	3747±9.70	1189±8.97	525±7.39	514±7.37	2209±3.52
Kidney	125±0.65	61±1.23	197±2.86	724±2.59	122±1.18	73±0.81	221±5.03	693±0.22
Stomach	50±1.40	19±0.43	43±0.98	270±1.61	40±1.65	18±0.33	46±0.27	247±4.12
Spine	322±5.32	150±2.81	296±5.15	1261±10.27	193±3.02	118±0.29	165±0.51	839±3.11
Bone	88±1.93	31±1.08	90±0.40	413±1.92	62±1.11	33±0.80	55±0.12	307±5.94
Fat Pad	121±1.67	50±6.33	172±1.57	588±11.38	116±2.75	20±1.43	121±2.81	612±14.15

Supporting Table 2. Organ biodistribution (%) of 4T1-PamGRET-DiR bEV and sEV at 0.5 H and 24 H post-injection.

Organ	Time	4T1-PalmGRET-DiR bEV				4T1-PalmGRET-DiR sEV			
		10 µg		25 µg		10 µg		25 µg	
		PalmGRET (520 nm)	DiR (800 nm)	PalmGRET (520 nm)	DiR (800 nm)	PalmGRET (520 nm)	DiR (800 nm)	PalmGRET (520 nm)	DiR (800 nm)
Brain	**0.5H**	4.84	2.01	1.02	0.69	4.15	3.10	0.2	1.80
	24H	0.34	0.33	0.1	0.91	0.06	0.50	0.12	1.53
Lung	**0.5H**	32.8	2.42	51.3	6.13	36.63	2.57	53.9	9.30
	24H	7.13	2.65	4.21	3.16	1.15	1.43	8.64	6.27
Heart	**0.5H**	0.99	0.68	6.96	0.32	4.37	1.08	14.78	1.81
	24H	0.26	0.09	0.18	0.28	0.07	0.13	0.95	0.68
Liver	**0.5H**	32.8	87.59	30.39	88.48	28.39	85.36	27.94	81.72
	24H	69.24	93.72	85.23	88.28	89.16	94.22	80.73	82.68
Spleen	**0.5H**	7.02	5.17	2.49	2.94	21.47	5.45	1.24	2.46
	24H	4.45	2.34	1.97	3.95	4.21	2.47	2.7	3.98
Kidney	**0.5H**	3.28	0.38	1.66	0.35	3.03	0.56	0.37	1.06
	24H	10.53	0.17	5.1	0.76	1.41	0.34	3.3	1.25
Stomach	**0.5H**	0.65	0.15	0.11	0.08	0.38	0.18	0.18	0.22
	24H	1.11	0.05	0.16	0.28	0.19	0.09	0.26	0.45
Spinal cord	**0.5H**	11.5	0.97	4.33	0.53	9.95	0.88	1.04	0.79
	24H	2.7	0.42	1.42	1.33	2.19	0.55	1.72	1.51
Bone	**0.5H**	2.65	0.27	0.68	0.16	2.9	0.29	0.14	0.27
	24H	0.94	0.09	0.76	0.43	1.3	0.16	0.87	0.55
Fat Pad	**0.5H**	3.47	0.37	1.04	0.31	3.74	0.53	0.22	0.58
	24H	3.31	0.14	0.87	0.62	0.26	0.10	0.71	1.10

Supporting Table 3. List of primers.

Target	**Forward**	**Reverse**
Cd44	TCGATTTGAATGTAACCTGCCG	CAGTCCGGGAGATACTGTAGC
Cd9	TGGGGCTATACCCACAAGGA	GCTTTGAGTGTTTCCCGCTG
Slc29a1	CAGCCTCAGGACAGGTATAAGG	GTTTGTGAAATACTTGGTTGCGG
Internal Control	**Forward**	**Reverse**
β-actin	TCCATCATGAAGTGTGACGT	TACTCCTGCTTGCTGATCCACAT

Supplementary Table 4. Organ biodistribution (%) of 4T1-PamGRET-Scramble, -shCd9, -shCd44, and -shSlc29a1 bEV and sEV.

Organ	10 µg Scramble				10 µg shCd9				10 µg shCd44				10 µg shSlc29a1			
	bEV		sEV		bEV		sEV		bEV		sEV		bEV		sEV	
	0.5H	72.5H	0.5H	72.5H	0.5H	72.5H	0.5H	72.5 H	0.5H	72.5H	0.5H	72.5H	0.5H	72.5H	0.5H	72.5H
Brain	0.46	0.48	0.37	0.31	0.19	0.44	0.36	0.37	0.49	0.46	0.40	0.39	0.35	0.38	0.25	0.34
Lung	24.06	31.71	22.98	33.74	28.46	18.16	21.63	23.25	14.49	16.27	14.18	17.41	16.80	16.43	12.79	17.55
Heart	0.93	1.25	0.74	1.02	0.76	1.24	0.98	0.88	1.26	1.41	1.07	1.49	0.80	1.24	0.69	1.08
Liver	21.30	9.30	23.54	15.72	17.89	12.25	23.78	16.35	22.01	11.15	23.47	15.40	21.97	14.22	32.56	18.62
Spleen	7.65	5.03	15.94	10.86	9.24	5.40	11.75	6.09	7.59	4.88	12.67	6.98	9.72	5.72	11.63	9.98
Kidney	7.47	10.04	5.58	6.76	8.08	12.24	6.41	8.48	11.78	11.15	8.55	9.84	12.42	11.17	7.82	8.81
Stomach	1.41	2.38	1.19	1.75	1.51	2.62	1.59	2.09	1.42	2.60	1.60	2.33	1.96	2.99	1.44	2.00
Spinal Cord	2.71	2.96	3.49	2.93	2.77	2.62	2.38	2.52	3.28	3.94	3.11	3.12	2.55	2.47	3.50	3.28
Bone	3.47	3.90	4.35	3.73	3.93	3.44	3.91	3.40	4.77	4.12	4.87	4.25	3.58	3.25	4.03	4.47
Fat Pad	1.71	2.35	1.21	1.53	1.92	2.18	1.37	1.88	2.26	2.57	2.05	2.45	1.52	2.47	1.53	2.14
Blood	28.83	30.60	20.60	21.65	25.24	39.42	25.84	34.71	30.64	41.44	28.04	36.35	28.33	39.65	23.75	31.73

Supporting Table 5. Organ biodistribution (%) of 4T1-PamGRET-Scramble, -shCd44 bEV and sEV at Days 0, 14, and 18 of EV treatment.

Organ	10 µg Scramble						10 µg shCd44					
	bEV			sEV			bEV			sEV		
	Day 0	Day 14	Day 18	Day 0	Day 14	Day 18	Day 0	Day 14	Day 18	Day 0	Day 14	Day 18
Brain	0.45	0.31	0.20	0.31	0.25	0.36	0.33	0.33	0.25	0.39	0.31	0.30
Lung	18.87	24.54	38.37	18.45	21.55	31.13	15.66	12.62	17.03	12.10	14.69	13.16
Heart	1.21	1.00	0.97	0.98	0.67	1.44	0.87	0.72	1.08	1.21	0.91	0.88
Liver	8.75	9.26	15.52	20.35	14.64	16.23	13.67	10.77	9.85	22.12	14.70	17.23
Spleen	5.50	5.86	6.53	14.41	19.16	13.08	4.46	3.99	4.46	7.68	7.35	6.03
Kidney	16.20	5.77	3.98	14.14	7.22	7.07	13.13	8.08	7.69	11.59	7.56	9.13
Stomach	1.34	3.54	2.40	0.96	1.89	1.96	1.67	2.02	2.03	2.03	2.63	1.85
Spinal Cord	2.45	2.92	1.95	1.71	2.59	2.83	2.20	1.76	2.95	2.98	2.32	2.61
Bone	3.52	3.50	3.39	3.09	3.31	7.48	3.20	2.94	3.36	3.86	4.07	3.47
Fat Pad	2.58	1.95	1.56	1.57	1.39	0.87	2.05	1.95	2.12	2.02	2.19	2.13
Blood	39.12	38.84	23.20	24.02	26.00	16.01	42.75	52.92	47.41	34.01	41.33	41.14
Tumor	0.00	2.51	1.93	0.00	1.31	1.56	0.00	1.90	1.78	0.00	1.96	2.08

Supporting Table 6. List of antibodies and working dilutions.

Primary Antibody	Host	Isotype	Species Reactivity	Manufacturer	Cat. No.	Experiment	Working dilution
GFP	Rabbit	IgG	Recombinant GFP	GeneTex	GTX113617	Dot Blot	1:5000
Cd9	Rabbit	IgG	Hum, Ms, Rat	ThermoFisher Scientific	MA531980	Western Blot	1:3000
Cd44	Rabbit	IgG	Hum, Ms, Rat	GeneTex	GTX102111	Western Blot	1:1000
Slc29a1	Mouse	IgG	Hum, Ms, Rat	Santa Cruz Biotechnology	sc-377283	Western Blot	1:200
Calnexin	Mouse	IgG	Hum, Ms, Rat	GeneTex	GTX629976	Western Blot	1:3000
Alix	Mouse	IgG	Hum, Ms, Rat	Santa Cruz Biotechnology	sc-53540	Western Blot	1:500
Cd81	Rabbit	IgG	Ms	Cell Signaling Technology	10037S	Western Blot	1:3000
GFP	Chicken	IgG	Recombinant GFP	GeneTex	GTX13970	IHC-IF	1:500
Secondary Antibody		**Host**	**Isotype**	**Manufacturer**	**Cat. No.**	**Experiment**	**Working dilution**
Rabbit IRDye-800CW		Goat	IgG	Abcam	ab216773	Western Blot	1:10000
Mouse IRDye-680RD		Goat	IgG	LiCor	926-68070	Western Blot	1:5000
Chicken Alexa Fluor568		Goat	IgG	ThermoFisher Scientific	A-11041	IHC-IF	1:1000